Electronic Supplementary Information for

Solution and surface-confined chloride anion template redox-active ferrocene catenanes

Nicholas H. Evans, Habibur Rahman, Alexandre V. Leontiev, Neil D. Greenham, Grzegorz A. Orlowski, Qiang Zeng, Robert M. J. Jacobs, Christopher J. Serpell, Nathan L. Kilah, Jason J. Davis* and Paul D. Beer*

Chemistry Research Laboratory, Department of Chemistry,
University of Oxford, 12 Mansfield Road, Oxford, OX1 3TA

Email: paul.beer@chem.ox.ac.uk

Contents

1) Experimental procedures

General considerations

Commerically available solvents and chemicals were used without further purification unless otherwise stated. Where dry solvents were used, they were degassed with nitrogen, dried by passing through a MBraun MPSP-800 column and then used immediately. Deionized water was used in all cases. NEt_3 was distilled from and stored over potassium hydroxide. Thionyl chloride was distilled from triphenyl phosphite. Grubbs' 2nd generation catalyst was stored in a desiccator.

NMR spectra were recorded on Varian Mercury 300, Varian Unity Plus 500 and Bruker AVII 500 (with ^{13}C Cryoprobe) spectrometers. Mass spectra were carried out on Waters Micromass LCT, Waters GCT, Bruker micrOTOF and Bruker FT-IR spectrometers. Melting points were recorded on a Gallenkamp capillary melting point apparatus and are uncorrected.

Compounds **2**.Cl,[1, 2] **ESI-3**,[3] and **ESI-4**.Cl,[4] were prepared according to literature procedures.

Synthesis of ferrocene-appended macrocycle 1

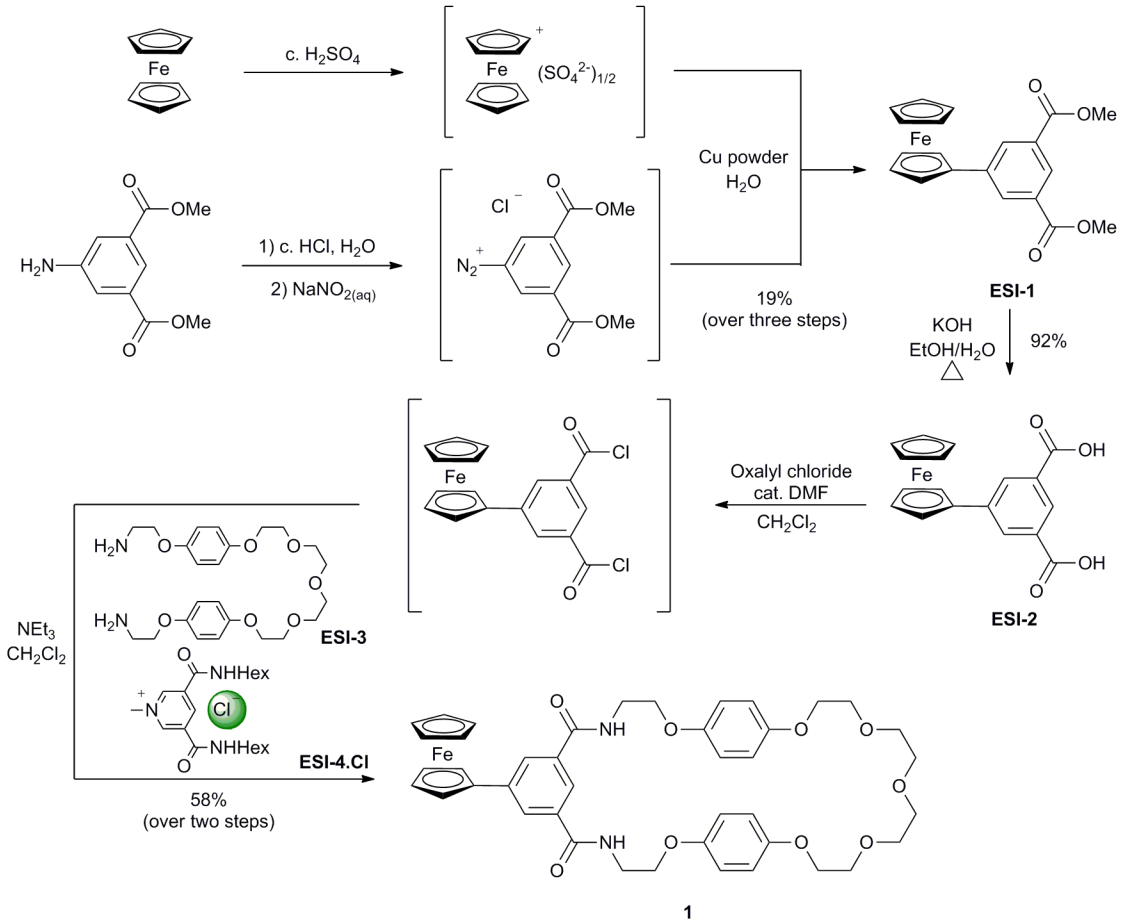

Supplementary Scheme 1: Synthesis of ferrocene-appended macrocycle **1**.

Dimethyl 5-ferrocenylisophthalate (ESI-1). Ferrocene (2.00 g, 10.8 mmol) was dissolved in conc. H_2SO_4 (30 mL), and stirred for 6 h. Meanwhile, dimethyl 5-aminoisophthalate (0.74 g, 3.5 mmol) was suspended in conc. HCl (10 mL) and H_2O (10 mL), and cooled to 0°C. A solution of $NaNO_2$ (1.00 g, 14.5 mmol) in H_2O (20 mL) was then added dropwise at 0°C. This solution was then stirred at 0°C for 1 h, and then used immediately. The ferrocenium solution was added to ice H_2O (120 mL) and allowed to warm to room temperature. Copper powder (1.00g, 15.7 mmol) was then added. This mixture was poured onto the diazonium ion solution, with the reaction mixture being stirred at 0°C for 30 min, then allowed to warm to room temperature and stirred for 60 h. Excess ascorbic acid (6.00 g) was then added, followed by CH_2Cl_2 (200 mL). This mixture was filtered through Celite® and washed thoroughly with CH_2Cl_2. The aqueous layer was extracted with CH_2Cl_2, with the combined organic layers dried ($MgSO_4$) and the solvent removed *in vacuo*. Silica gel chromatography (CH_2Cl_2) yielded the product as an orange solid (0.26 g, 19%): mp 160°C; δ_H(300 MHz; $CDCl_3$) 8.48 (1H, t, ^4J = 1.7 Hz, Ar*H*^{2}), 8.29 (2H, d, ^4J = 1.7 Hz, Ar*H*^{4} & Ar*H*^{6}), 4.78 (2H, t, ^3J = 1.9 Hz, Cp*H*), 4.40 (2H, t, ^3J = 1.9 Hz, Cp*H*), 4.06 (5H, s, Cp'*H*), 3.99 (6H, s, C*H*$_3$); δ_C(75.5 MHz; $CDCl_3$) 166.4, 141.0, 130.8, 127.7, 82.8, 69.7, 69.7 (sic), 66.7, 52.4; *m/z* (ES) 378.0546 $[M]^+$ ($C_{20}H_{18}FeO_4$ requires 378.0549).

5-Ferrocenylisophthalic acid (ESI-2). To **ESI-1** (245 mg, 0.65 mmol) suspended in EtOH (25 mL) was added an aqueous solution of KOH (182 mg, 3.24 mmol in 2.5 mL of H_2O) which was subsequently heated under reflux for 16 h. The reaction was allowed to cool to room temperature, the volume of solvent reduced by 50%, then aqueous 10% citric acid added to achieve pH 5. H_2O (25 mL) was added, and the resulting orange precipitate was collected by filtration, washed with H_2O and dried rigorously under vacuum to yield the product (209 mg, 92%): mp > 240°C (dec.); δ_H(300 MHz; d_6-DMSO) 8.30 (1H, t, ^4J = 1.5 Hz, Ar*H*^{2}), 8.16 (2H, d, ^4J = 1.5 Hz, Ar*H*^{4} & Ar*H*^{6}), 4.84 (2H, t, ^3J = 1.8 Hz, Cp*H*), 4.40 (2H, t, ^3J = 1.8 Hz, Cp*H*), 4.03 (5H, s, Cp'*H*); δ_C(75.5 MHz; d_6-DMSO) 168.0, 138.6, 135.0, 128.8, 127.8, 84.1, 69.4, 69.2, 66.4; *m/z* (ES) 349.0164 $[M - H]^-$ ($C_{18}H_{13}FeO_4$ requires 349.0169). This data is consistent with previously reported literature values.[5]

Ferrocene-appended macrocycle 1. To a suspension of **ESI-2** (150 mg, 0.428 mmol) suspended in dry CH_2Cl_2 (10 mL) at 0°C was added oxalyl chloride (544 mg, 363 μL, 4.28 mmol) and dry DMF (a drop, catalytic). The reaction mixture was then stirred at room temperature for 16 hours under a N_2 atmosphere. The solvent was subsequently removed *in vacuo*, and the diacid chloride was added as a CH_2Cl_2 (5 mL) solution via a dropping funnel to a solution of bis-amine **ESI-3** (199 mg, 0.428 mmol) and template **ESI-4**.Cl (164 mg, 0.428 mmol) in CH_2Cl_2 (20 mL) immediately after the addition of NEt_3 (108 mg, 149 μL, 1.07 mmol). This reaction mixture was stirred under a N_2 atmosphere for 1 hour, then washed with 1 M citric acid (2 × 25 mL) and H_2O (1 × 25 mL), the organic dried ($MgSO_4$) and solvent removed, the crude material being purified by silica gel chromatography (CH_2Cl_2:CH_3OH 98:2) to yield the product as an orange solid (162 mg, 49%): mp 152°C; δ_H(300 MHz; $CDCl_3$:CD_3CN 1:1) 7.95 (1H, s, Ar*H*^{2}), 7.79 (2H, s, Ar*H*^{4} & Ar*H*^{6}), 7.25 (2H, t, ^3J = 5.1 Hz, N*H*), 6.75-6.84 (8H, m, hydroquinone Ar*H*), 5.00 (2H, br. s, Cp*H*), 4.57 (2H, br. s, Cp*H*), 4.21 (5H, br. s, Cp'*H*), 4.98 (4H, t, ^3J = 5.0 Hz, C*H*$_2$), 3.96-4.00 (4H, m, C*H*$_2$) 3.74-3.79 (8H, m, 2 × C*H*$_2$), 3.59-3.64 (8H, m, 2 × C*H*$_2$); δ_C(125.8 MHz; $CDCl_3$:CD_3CN 1:1) 167.1, 153.7, 153.4, 141.5, 135.1, 128.3, 122.3, 116.0, 115.8, 71.0, 70.1, 68.5, 67.5, 40.1 (1 peak missing); *m/z* (ES) 801.2425 $[M + Na]^+$ ($C_{42}H_{46}FeN_2NaO_9$ requires 801.2446).

Synthesis of ferrocene-appended catenanes 3.X (X^- = Cl^-, PF_6^-) and **4**.$(Cl)_2$

Chloride salt of ferrocene-appended [2]catenane 3.Cl**.** Macrocycle **1** (75.0 mg, 0.096 mmol) and RCM precursor **2**.Cl (63.2 mg, 0.096 mmol) were dissolved in dry CH_2Cl_2 (25 mL) and stirred for 20 minutes under a N_2 atmosphere. Grubbs' 2nd generation catalyst (6.3 mg, 10% by wt) added and the reaction stirred under N_2 atmosphere for 16 h. The solvent was removed *in vacuo* and the crude reaction mixture purified by silica gel prep TLC (CH_2Cl_2:CH_3OH 97:3) to yield the product as an orange solid (46 mg, 34%): mp 230°C (dec.); δ_H(300 MHz; $CDCl_3$) 9.63 (1H, s, *para*-pyridinium Ar*H*), 8.94 (1H, s, isophthalamide ArH^2), 8.82 (2H, s, *ortho*-pyridinium Ar*H*), 8.70 (1H, s, isophthalamide N*H*), 8.63 (2H, s, pyridinium N*H*), 8.50 (1H, s, isophthalamide N*H*'), 8.39 (1H, s, *ortho*-isophthalamide Ar*H*), 8.28 (1H, s, *ortho*-isophthalamide Ar*H*'), 6.72-6.82 (8H, m, isophthalamide hydroquinone Ar*H*), 6.40-6.42 (2H, m, pyridinium hydroquinone Ar*H*), 6.11-6.17 (4H, m, pyridinium hydroquinone Ar*H*), 6.02-6.04 (2H, m, pyridinium hydroquinone Ar*H*), 5.84 (2H, app. s, C*H*=C*H*), 4.86 (2H, app. s, Cp*H*), 4.68 (3H, s, N^+CH_3), 3.24-4.48 (51H, m, Cp*H*, Cp'*H* & 11 × CH_2); δ_C(125.8 MHz; $CDCl_3$) 167.2,* 166.5,* 159.8 (3 carbonyl resonances), 153.8, 152.8, 152.7, 151.8, 151.5, 144.5, 140.8, 135.8, 134.0, 133.4, 129.5, 128.9, 121.4, 116.1, 114.7, 114.5 (16 isophthalamide, pyridinium, hydroquinone, alkene resonances), 84.1, 71.2, 70.6, 70.0 (very broad), 68.7, 68.4, 68.1, 67.1, 66.4, 65.5, 64.4, 49.9 (12 Fc, *C*O and N^+CH_3 resonances observed – at least 2 coincident resonances), 41.4,* 41.2,* 39.9 (3 *C*NH resonances), * = assignable evidence of asymmetry by doubling of carbonyl and *C*NH resonances; *m/z* (ES) 1370.5250 $[M - Cl]^+$ ($C_{74}H_{84}FeN_5O_{17}$ requires 1370.5209).

Hexafluorophosphate salt of ferrocene-appended [2]catenane 3.PF_6**. 3**.Cl (36 mg, 0.026 mmol) dissolved in $CHCl_3$ (10 mL) was washed with 0.1 M NH_4PF_6 (10 × 10 mL), then H_2O (3 × 10 mL). The organic layer was dried ($MgSO_4$) and the solvent removed *in vacuo* to give the product as an orange film (32 mg, 88%): mp > 200°C (dec.); δ_H(300 MHz, $CDCl_3$) 9.04 (1H, s, *para*-pyridinium Ar*H*), 8.38 (2H, s, *ortho*-pyridinium Ar*H*), 8.25 (2H, s, isophthalamide ArH^4 & ArH^6), 8.15 (1H, s, isophthalamide ArH^2), 8.02 (2H, t, ^3J = 4.4 Hz, pyridinium N*H*), 7.27 (2H, br. s, isophthalamide N*H*), 6.74-6.77 (4H, m, pyridinium hydroquinone Ar*H*), 6.66-6.69 (4H, m, pyridinium hydroquinone Ar*H*), 6.54-6.57 (4H, d, ^3J = 8.8 Hz, isophthalamide hydroquinone Ar*H*), 6.31-6.34 (4H, d, ^3J = 8.8 Hz, isophthalamide hydroquinone Ar*H*), 5.87 (2H, br. s, C*H*=C*H*), 4.88 (2H, s, Fc Cp*H*), 4.42 (2H, s, Fc Cp*H*), 3.57-4.10 (52H, m, Fc Cp'*H* & N^+CH_3 & 10 × CH_2); δ_C(125.8 MHz; $CDCl_3$) 167.1, 160.8, 153.3, 153.1, 152.4, 151.6, 145.0, 141.0, 140.5, 134.5, 133.6, 128.9, 128.5, 121.1, 115.7, 115.3, 115.1, 114.5, 83.5, 71.1, 70.6, 70.3, 70.0, 69.8, 69.6, 69.1, 68.3, 67.2, 66.8, 66.5, 66.3, 49.6, 40.6, 39.8; δ_F(282.4 MHz; $CDCl_3$) -70.7 (d, ^1J = 714 Hz, PF_6^-); δ_P(121.5 MHz; $CDCl_3$) -144.0 (septet, ^1J = 714 Hz, *P*F_6^-); *m/z* (ES) 1370.5260 $[M - PF_6]^+$ ($C_{74}H_{84}FeN_5O_{17}$ requires 1370.5209).

Chloride salt of ferrocene-appended [3]catenane 4.$(Cl)_2$**.** This was recovered as an orange solid as a by-product from the reaction to form [2]catenane **3**.Cl (yield < 5%): mp > 200°C (dec); δ_H(300 MHz; $CDCl_3$) 9.63 (2H, s, *para*-pyridinium Ar*H*), 8.92 (2H, s, isophthalamide ArH^2), 8.82 (4H, s, *ortho*-pyridinium Ar*H*), 8.70 (4H, app. s, pyridinium N*H*), 8.64 (4H, app. s, isophthalamide N*H*), 8.27 (2H, s, *ortho*-isophthalamide Ar*H*), 6.79 (16H, s, isophthalamide hydroquinone Ar*H*), 6.31 (8H, d, ^3J = 8.5 Hz, pyridinium hydroquinone Ar*H*), 6.05 (8H, d, ^3J = 8.5 Hz, pyridinium hydroquinone Ar*H*), 5.84 (4H, app. s, C*H*=C*H*), 4.78 (4H, s, Cp*H*), 4.64 (6H, s,

N^+CH_3), 4.34 (4H, s, Cp*H*), 4.01-4.08 (42H, m, Fc Cp'*H* & 4 × CH_2), 3.71-3.74 (56H, m, 7 × CH_2); δ_C(125.8 MHz; $CDCl_3$) 166.9, 159.9, 153.8, 153.1, 152.6, 151.6, 144.5, 140.8, 133.8, 133.2, 129.5, 128.8, 121.4, 115.6, 115.1, 114.4, 114.3, 83.7, 71.2, 70.6, 70.5, 70.0, 69.7, 69.3, 68.6, 68.2, 68.0, 66.8, 66.5, 64.9, 49.7, 41.2, 39.9 (one Ar*C* resonance not observed); *m/z* (ES) 1370.5195 ($[M - 2Cl]^{2+}$, $C_{148}H_{168}Fe_2N_{10}O_{34}$ requires 1370.5206).

Synthesis of *N*-methyl pyridinium bis-thiol thread 5.Cl

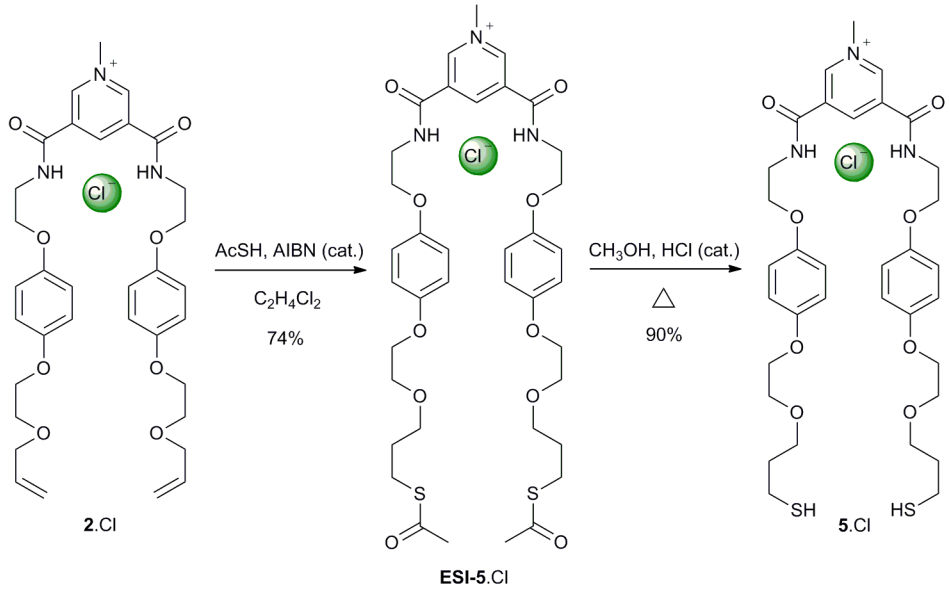

Supplementary Scheme 2: Synthesis of *N*-methyl pyridinium bis-thiol thread **5**.Cl.

Bis-acyl thiol thread ESI-5.Cl**.** A solution of RCM precursor **2.**Cl (60 mg, 0.09 mmol), thioacetic acid (213 mg, 0.2 mL, 2.8 mmol) and AIBN (45 mg, 0.28 mmol) in $C_2H_4Cl_2$ (0.2 mL) was degassed by bubbling gently $N_{2(g)}$ for 10 min then heated at 80°C for 3 h. The reaction mixture was cooled to room temperature and treated with hexane (5 mL) which led to precipitation of a yellow oil. The solution was decanted and the residue washed with hexane (5 × 5 mL) to remove the excess thioacetic acid. The remaining residue was purified by silica gel column chromatography (CH_2Cl_2:CH_3OH 85:15) giving the product as a yellow solid (0.055 g, 74%): mp 75-77°C; δ_H(300 MHz; $CDCl_3$) 10.25 (1H, s, *para*-pyridinium Ar*H*), 9.55 (2H, br. s, N*H*), 9.47 (2H, s, *ortho*-pyridinium Ar*H*), 6.63-6.85 (8H, m, hydroquinone Ar*H*), 4.45 (3H, s, N^+CH_3), 4.12 (4H, t, ^3J = 5.3 Hz, CH_2), 3.92-4.03 (4H, m, CH_2), 3.63-3.92 (8H, m, 2 × CH_2), 3.56 (4H, t, ^3J = 6.2 Hz, CH_2), 2.94 (4H, t, ^3J = 7.2 Hz, CH_2), 2.30 (6H, s, CH_3), 1.75-1.96 (4H, m, CH_2); δ_C(75.5 MHz; $CDCl_3$) 196.0, 160.6, 153.0, 152.7, 146.3, 141.7, 133.8, 115.8, 115.4, 69.8, 69.4, 68.0, 66.5, 49.1, 40.3, 30.6, 29.6, 26.0; *m/z* (ES) 772.2936 ($[M - Cl]^+$, $C_{38}H_{50}N_3O_{10}S_2$ requires 772.2932.

Bis-thiol thread 5.Cl**. ESI-5**.Cl (50 mg, 0.062 mmol) was dissolved in CH_3OH (3 mL) with a drop of conc. $HCl_{(aq)}$. The reaction mixture was refluxed under a N_2 atmosphere until the starting material had been consumed, as monitored by ESMS (approximately 8 h). After the solvent was removed, the residue was purified by silica gel column chromatography (CH_2Cl_2:CH_3OH 85:15) to give the product as a yellow

sticky solid (42 mg, 90%): δ_H(300 MHz; $CDCl_3$:CD_3OD 9:1) 9.47 (1H, s, *para*-pyridinium), 9.27 (2H, s, *ortho*-pyridinium Ar*H*), 9.11 (2H, br. s, N*H*), 6.63-6.85 (8H, m, Ar*H*), 4.41 (3H, s, N^+CH_3), 3.87-4.22 (8H, m, 2 × CH_2), 3.58-3.87 (8H, m, 2 × CH_2), 3.56 (4H, d, ^3J = 6.1 Hz, CH_2), 2.56 (4H, quart., ^3J = 7.1 Hz, CH_2), 1.66-1.91 (4H, m, CH_2), 1.35 (2H, t, ^3J = 8.0 Hz, S*H*); δ_C(75.5 MHz; $CDCl_3$:CD_3OD 9:1) 153.1, 152.7, 146.1, 141.9, 134.4, 115.6, 115.5, 69.4, 69.2, 67.9, 66.4, 40.3, 40.2, 33.5, 21.3, 21.1; *m/z* (ES) 688.2721 $[M - Cl]^+$, $C_{34}H_{46}N_3O_{10}S_2$ requires 688.2721.

2) Spectral characterization

Bis-ester **ESI-1**

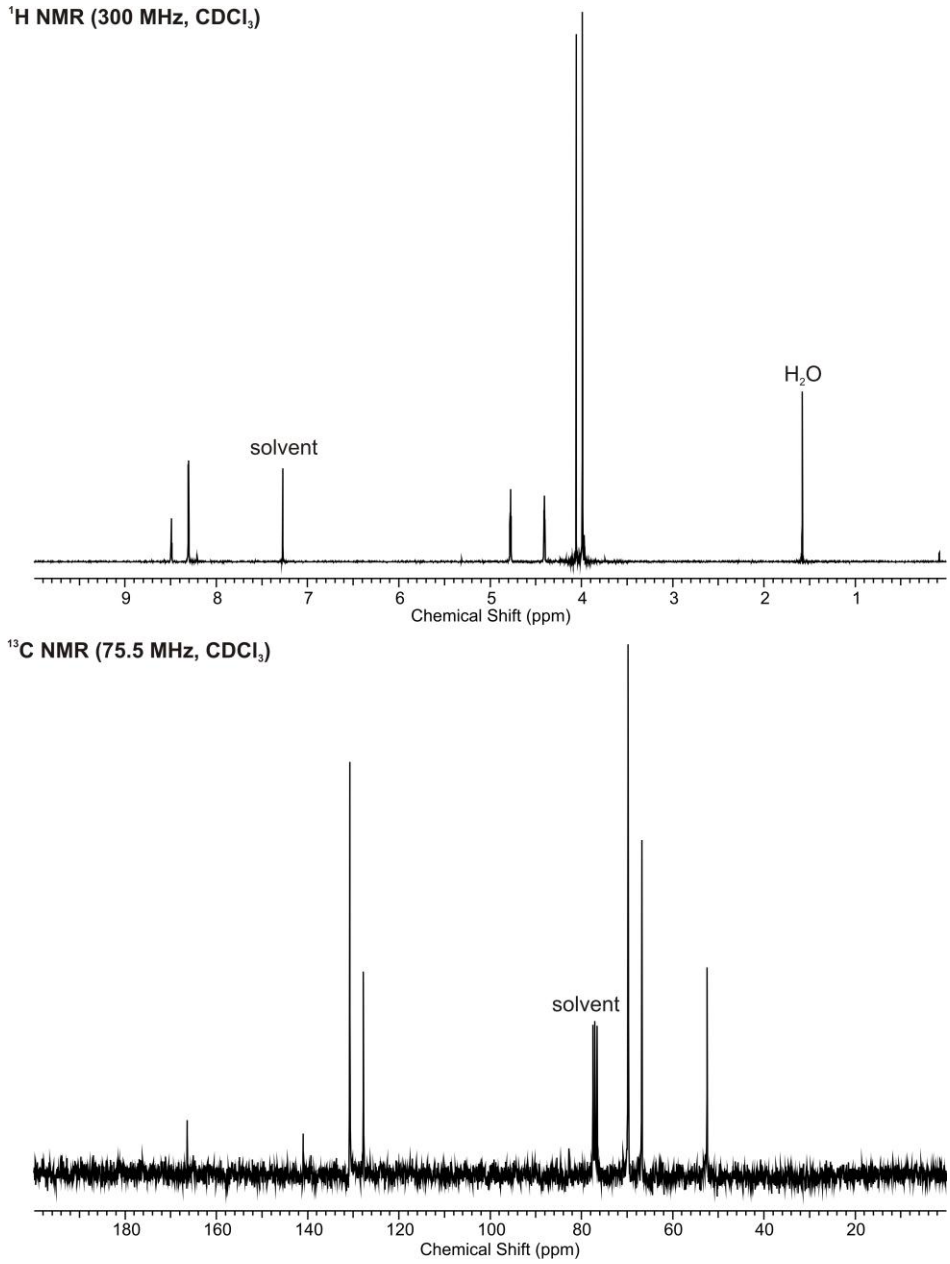

Supplementary Figure 1: ^{1}H and ^{13}C NMR spectra of bis-ester **ESI-1**.

Bis-acid **ESI-2**.

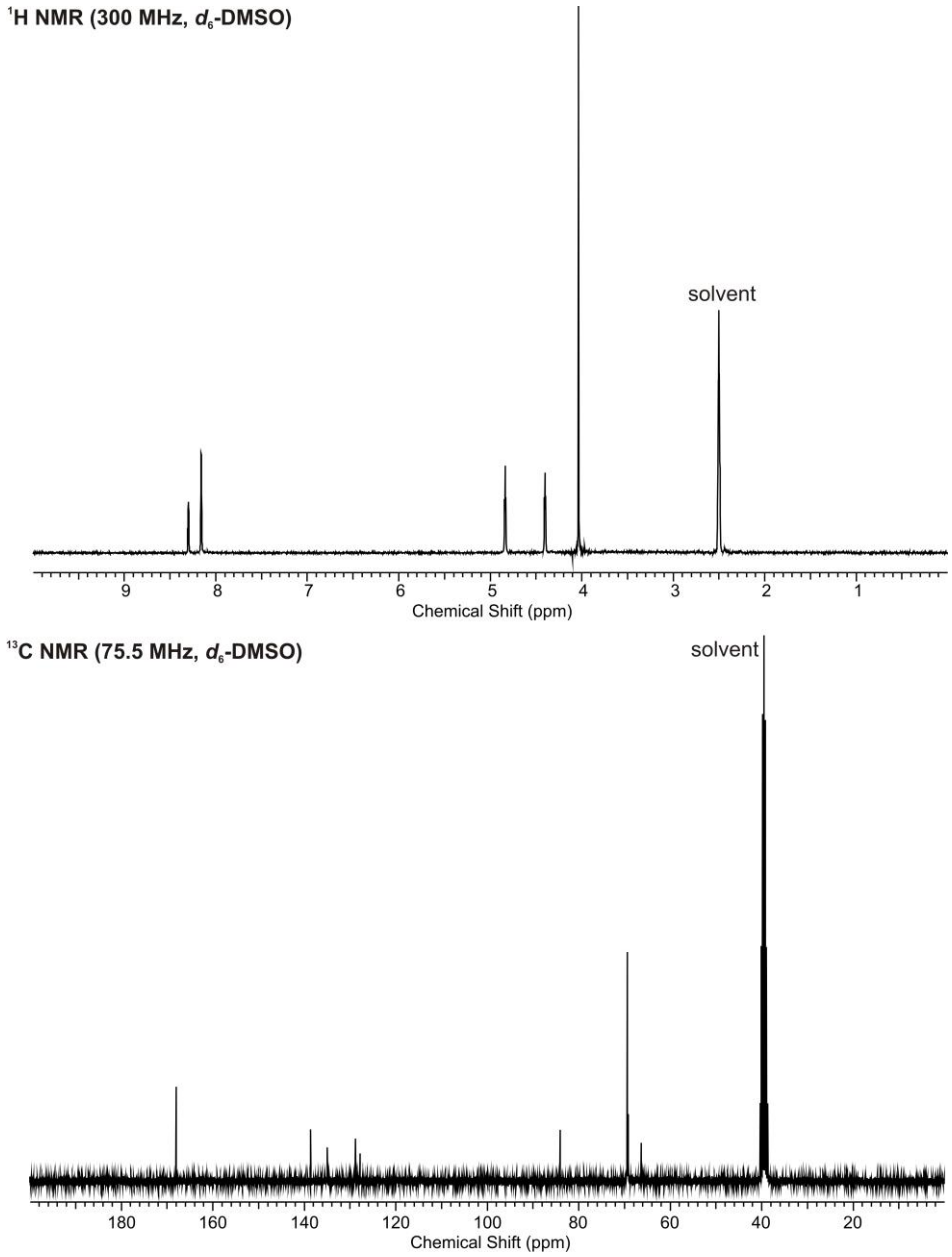

Supplementary Figure 2: ^{1}H and ^{13}C NMR spectra of bis-acid **ESI-2**.

Macrocycle **1**.

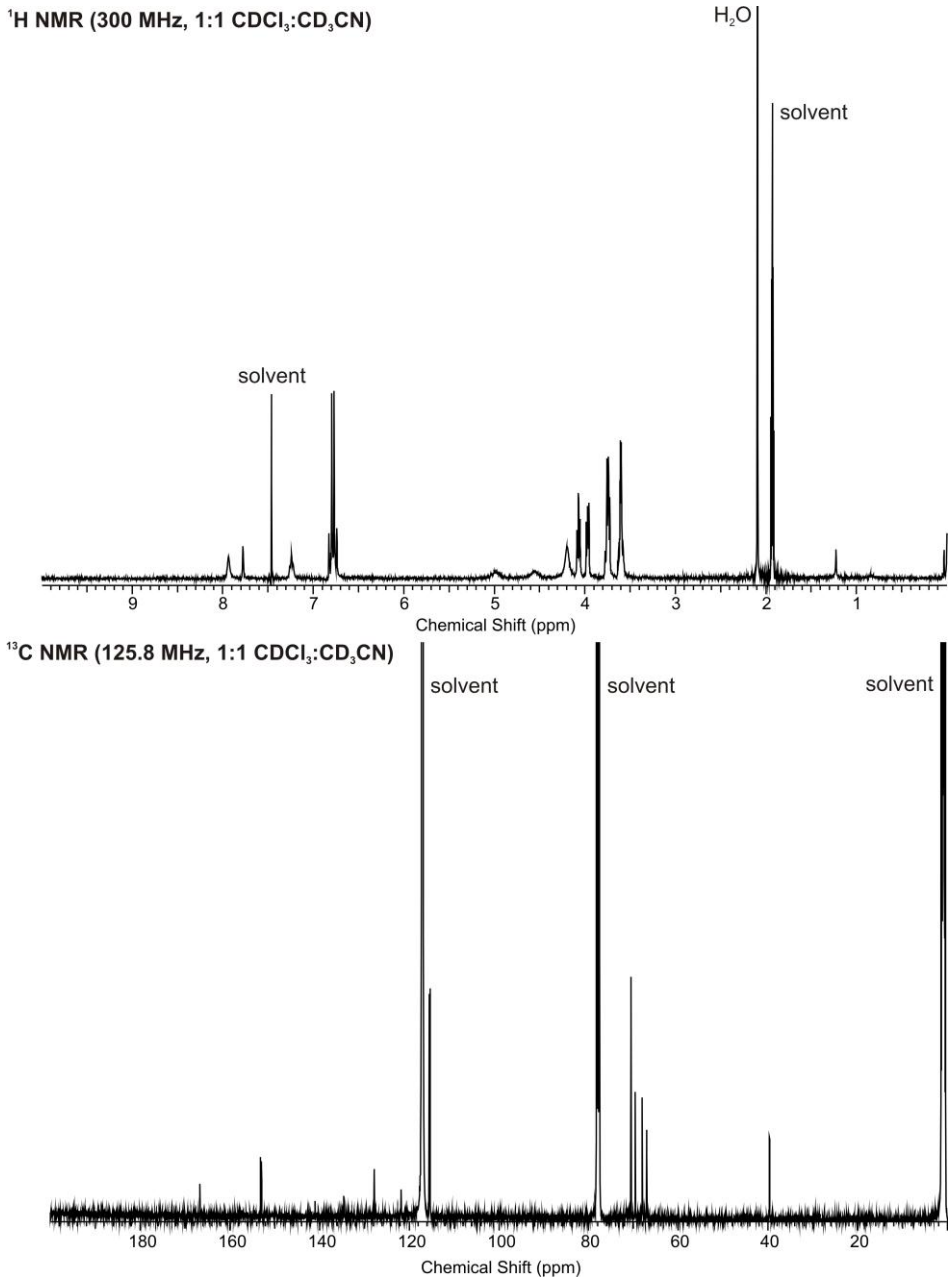

Supplementary Figure 3: ^{1}H and ^{13}C NMR spectra of macrocycle **1**.

[2]Catenane **3**.Cl

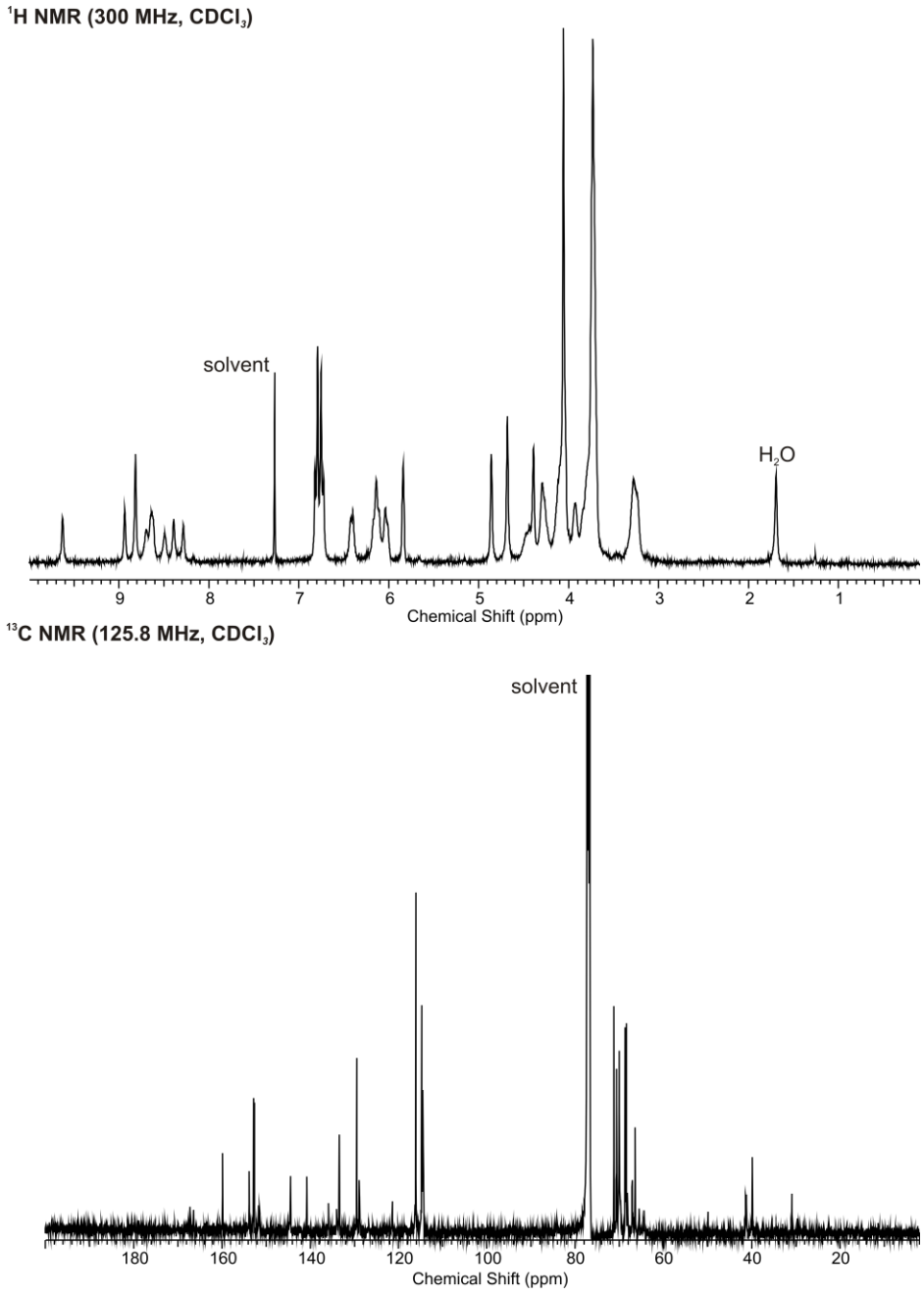

Supplementary Figure 4: ^{1}H and ^{13}C NMR spectra of [2]catenane **3**.Cl.

[2]Catenane **3**.Cl (cont.)

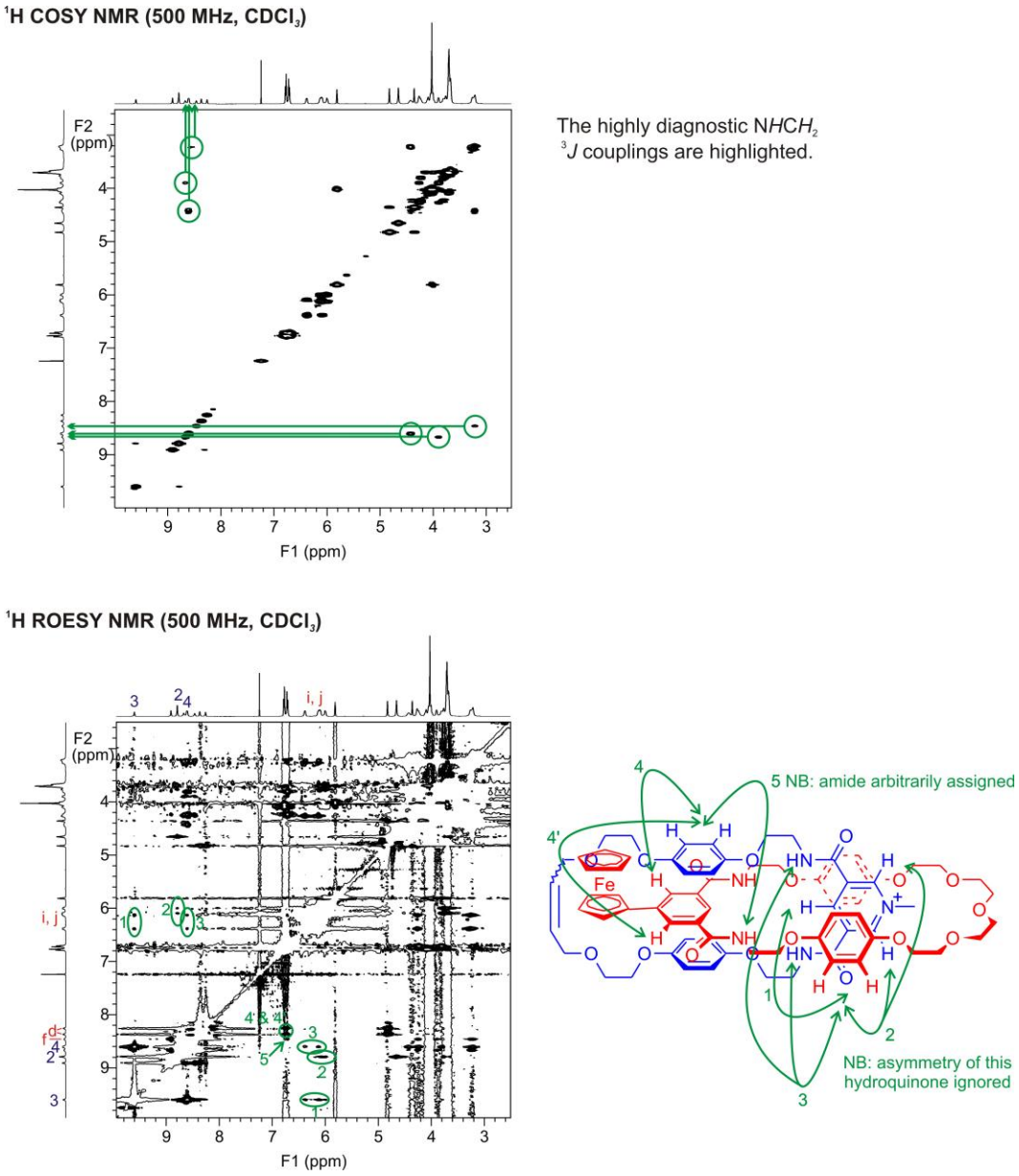

Supplementary Figure 5: ^{1}H COSY and ROESY NMR spectra of [2]catenane **3**.Cl

[2]Catenane **3**.Cl (cont.)

HR (ES +ve) MS

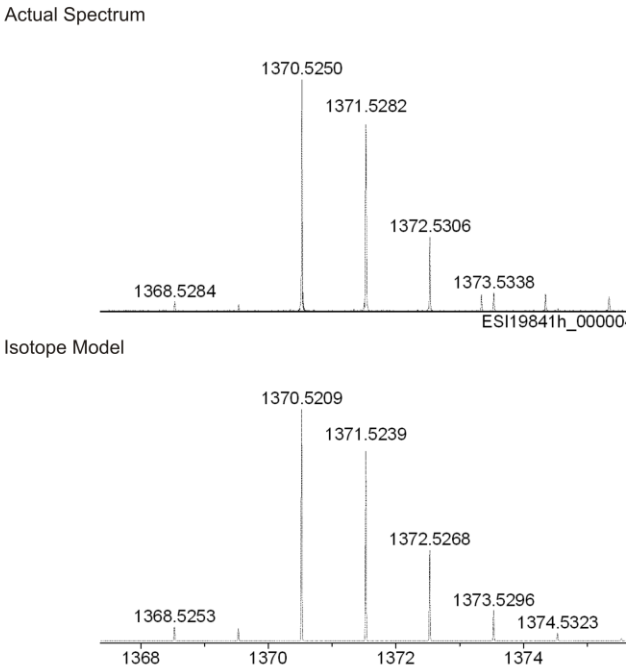

Supplementary Figure 6: HR mass spectrum of [2]catenane **3**.Cl

[2]Catenane **3**.PF_6.

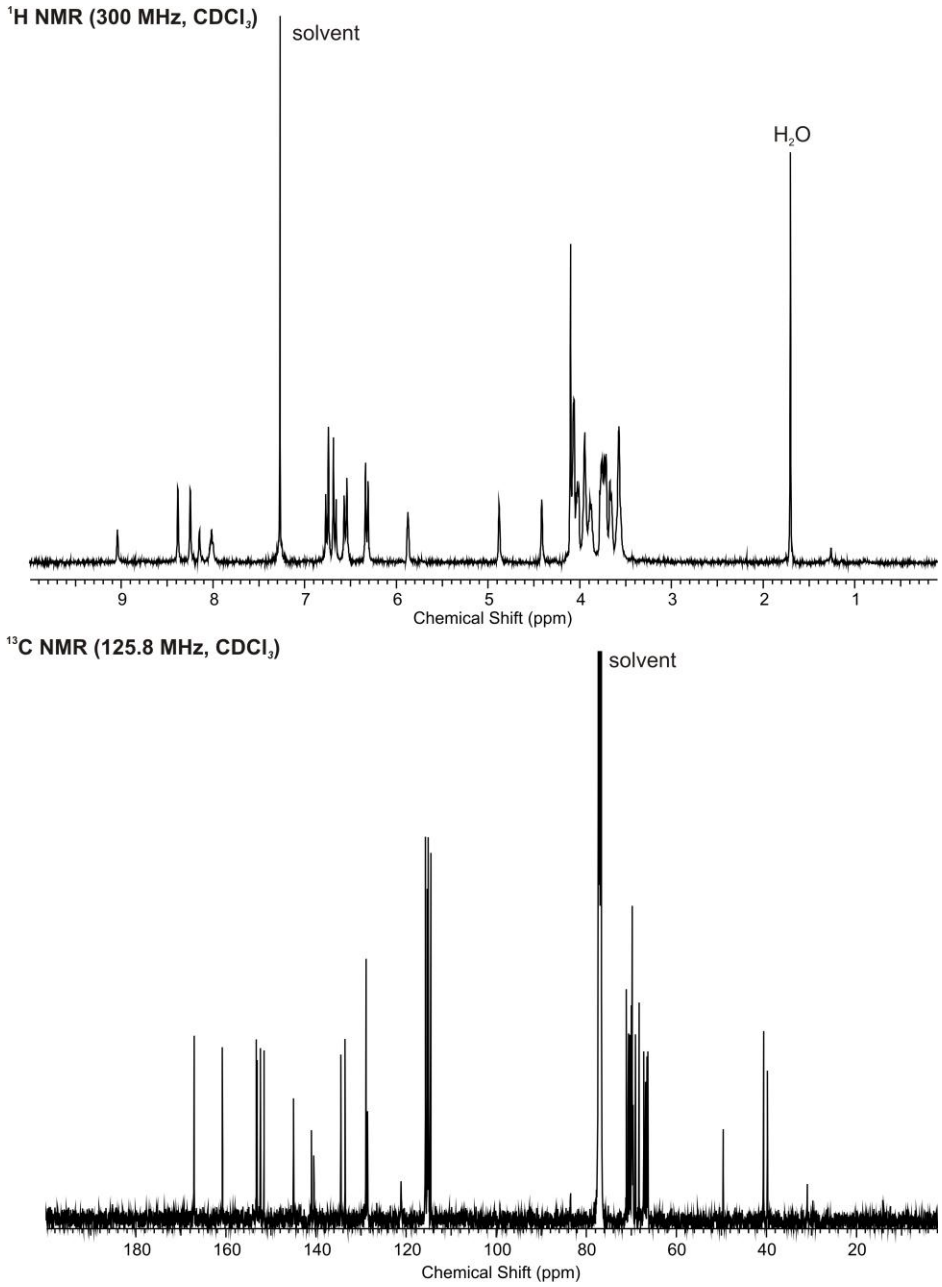

Supplementary Figure 7: ^{1}H and ^{13}C NMR spectra of [2]catenane **3**.PF_6.

[2]Catenane **3**.PF_6 (cont.)

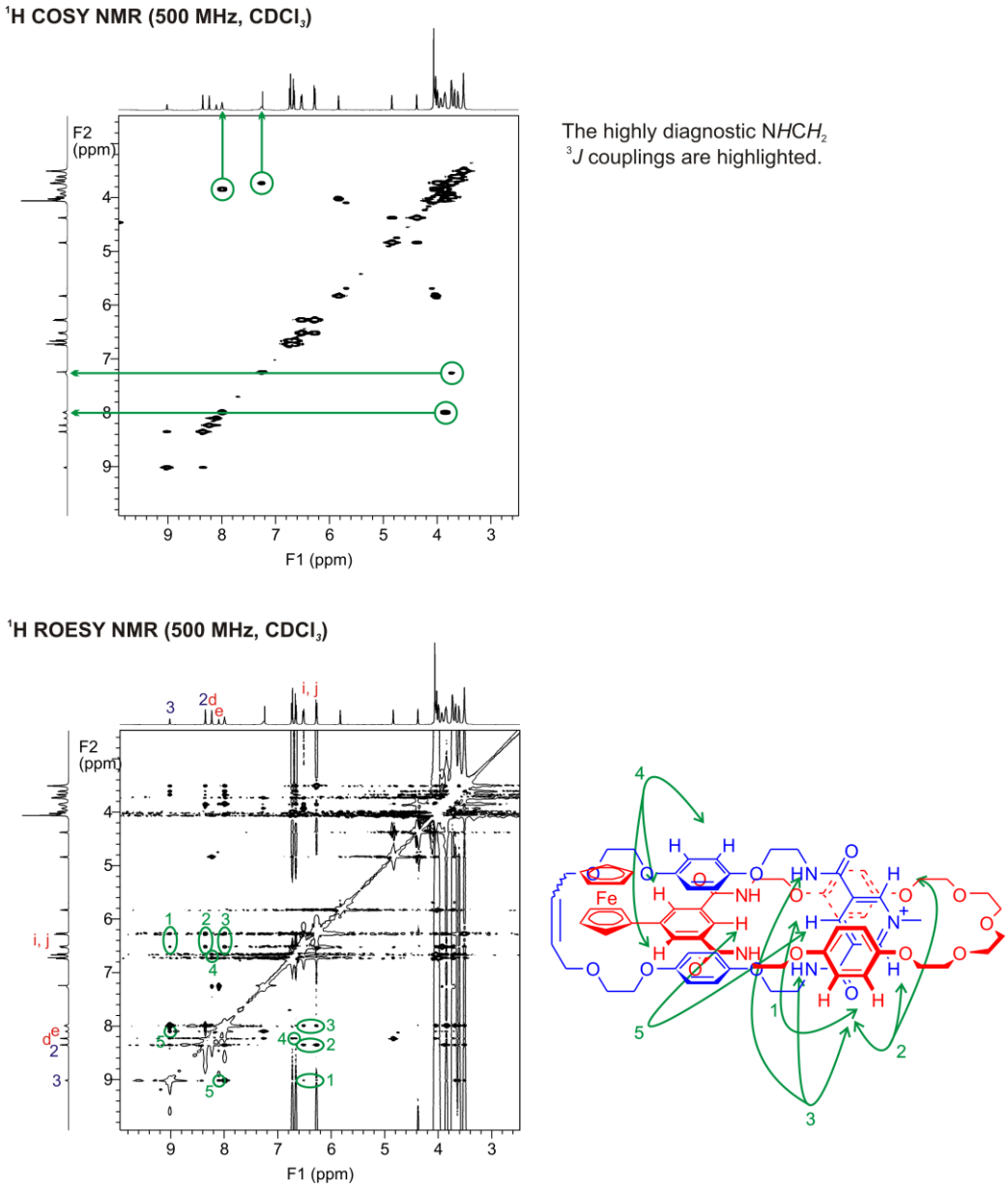

Supplementary Figure 8: ^{1}H COSY and ROESY NMR spectra of [2]catenane **3**.PF_6.

[2]Catenane **3**.PF_6 (cont.)

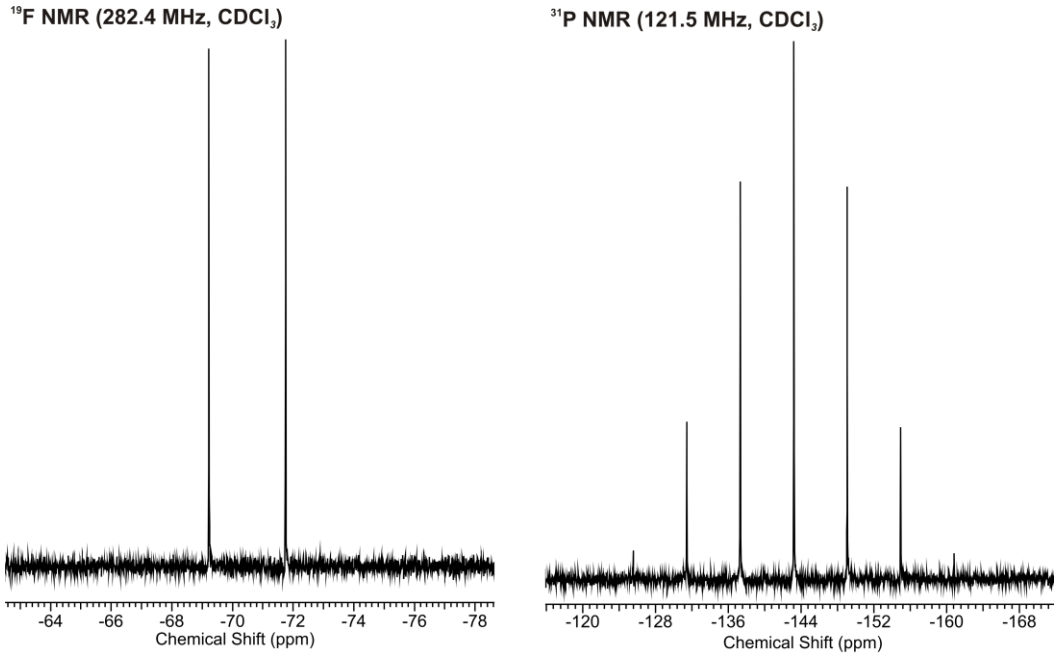

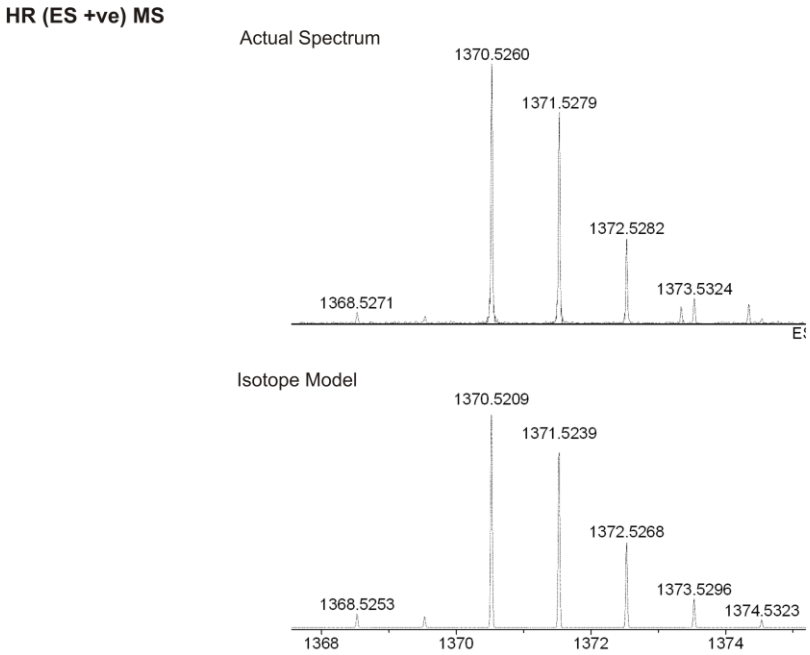

Supplementary Figure 9: ^{19}F and ^{31}P NMR and HR mass spectra of [2]catenane **3**.PF_6.

[3]Catenane **4**.$(Cl)_2$.

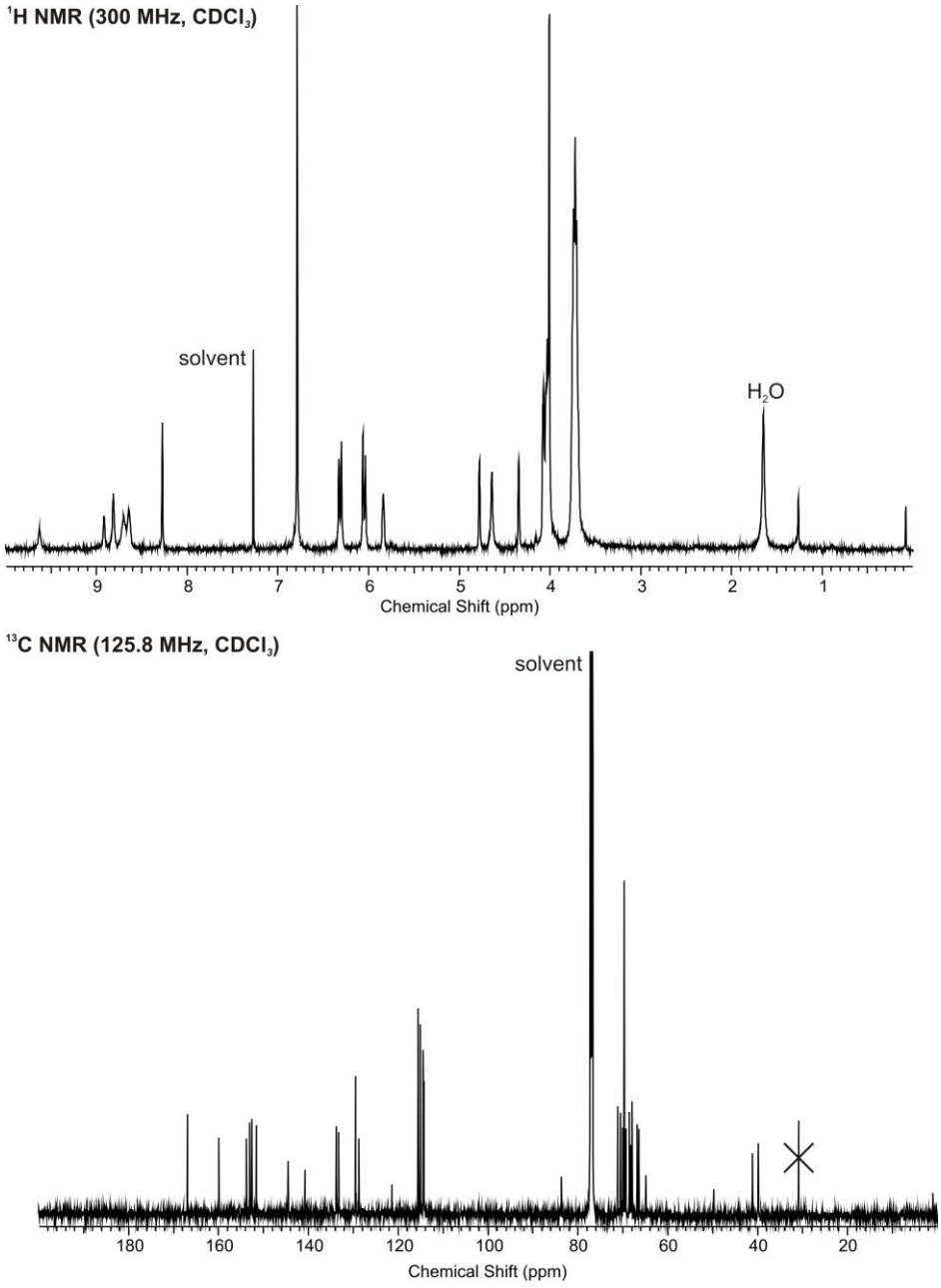

Supplementary Figure 10: ^{1}H and ^{13}C NMR spectra of [3]catenane **4**.$(Cl)_2$.

[3]Catenane **4**.$(Cl)_2$ (cont.)

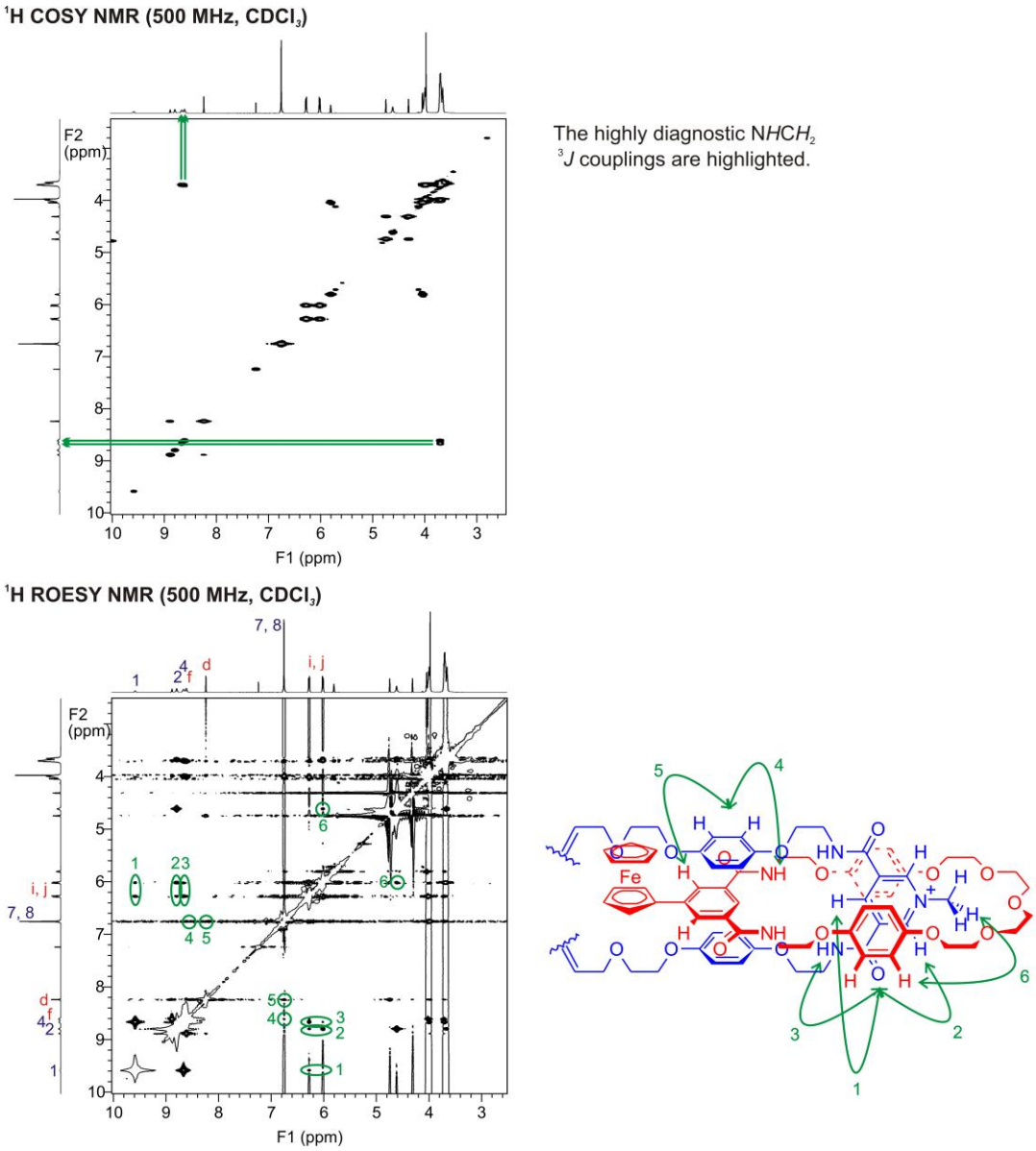

Supplementary Figure 11: ^{1}H COSY and ROESY NMR spectra of [3]catenane **4**.$(Cl)_2$.

[3]Catenane **4**.$(Cl)_2$ (cont.)

HR (ES +ve) MS

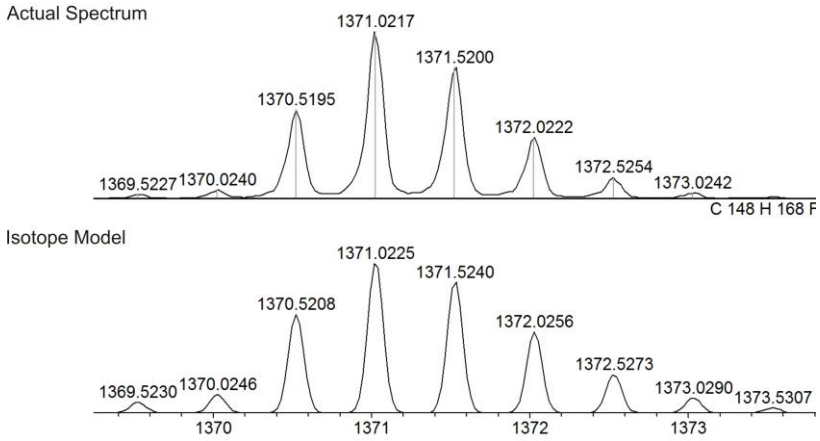

Supplementary Figure 12: HR mass spectra of [3]catenane **4**.$(Cl)_2$.

Bis-acyl thiol **ESI-5**.Cl.

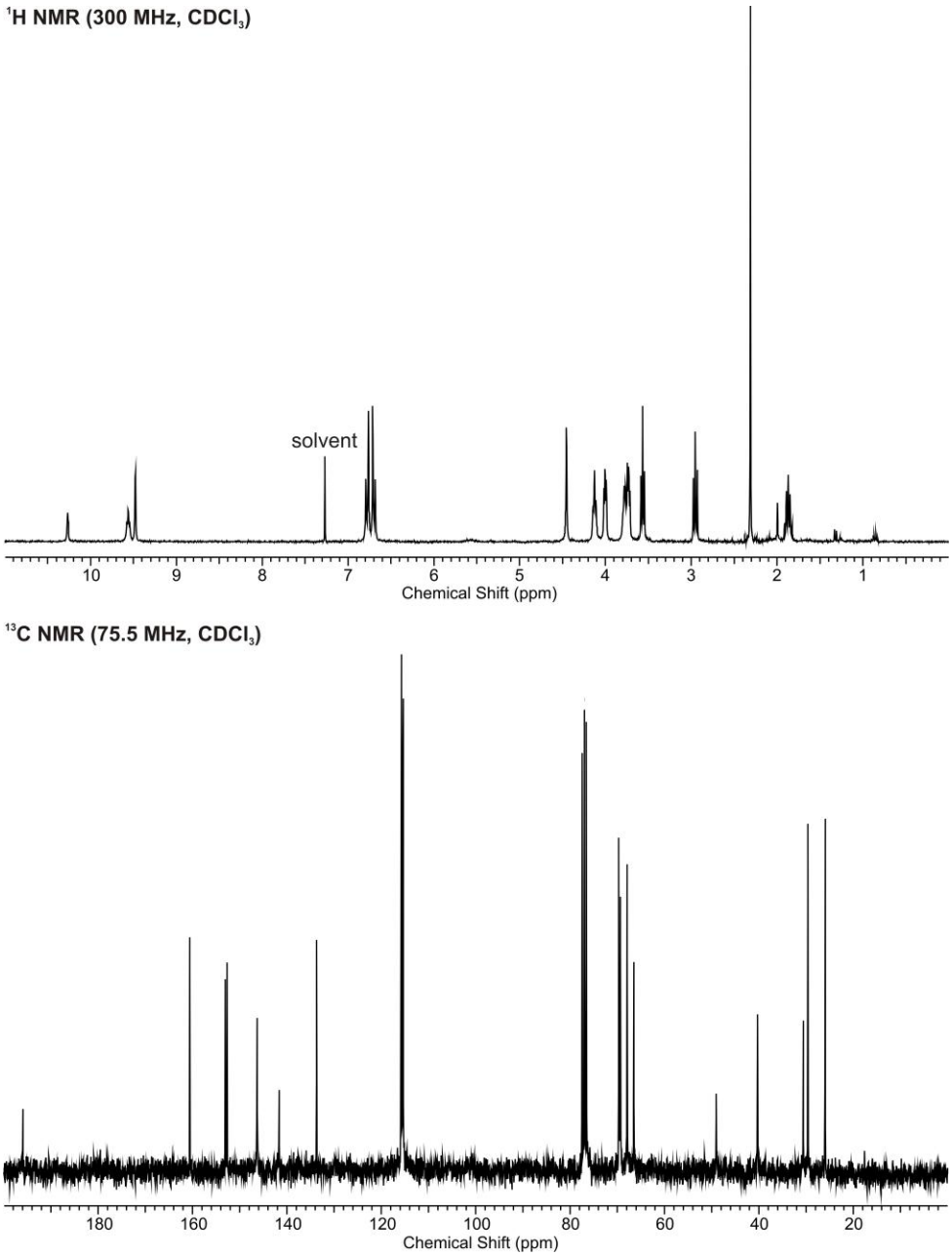

Supplementary Figure 13: ^{1}H and ^{13}C NMR spectra of bis-acyl thiol **ESI-5**.Cl.

Bis-thiol **5**.Cl.

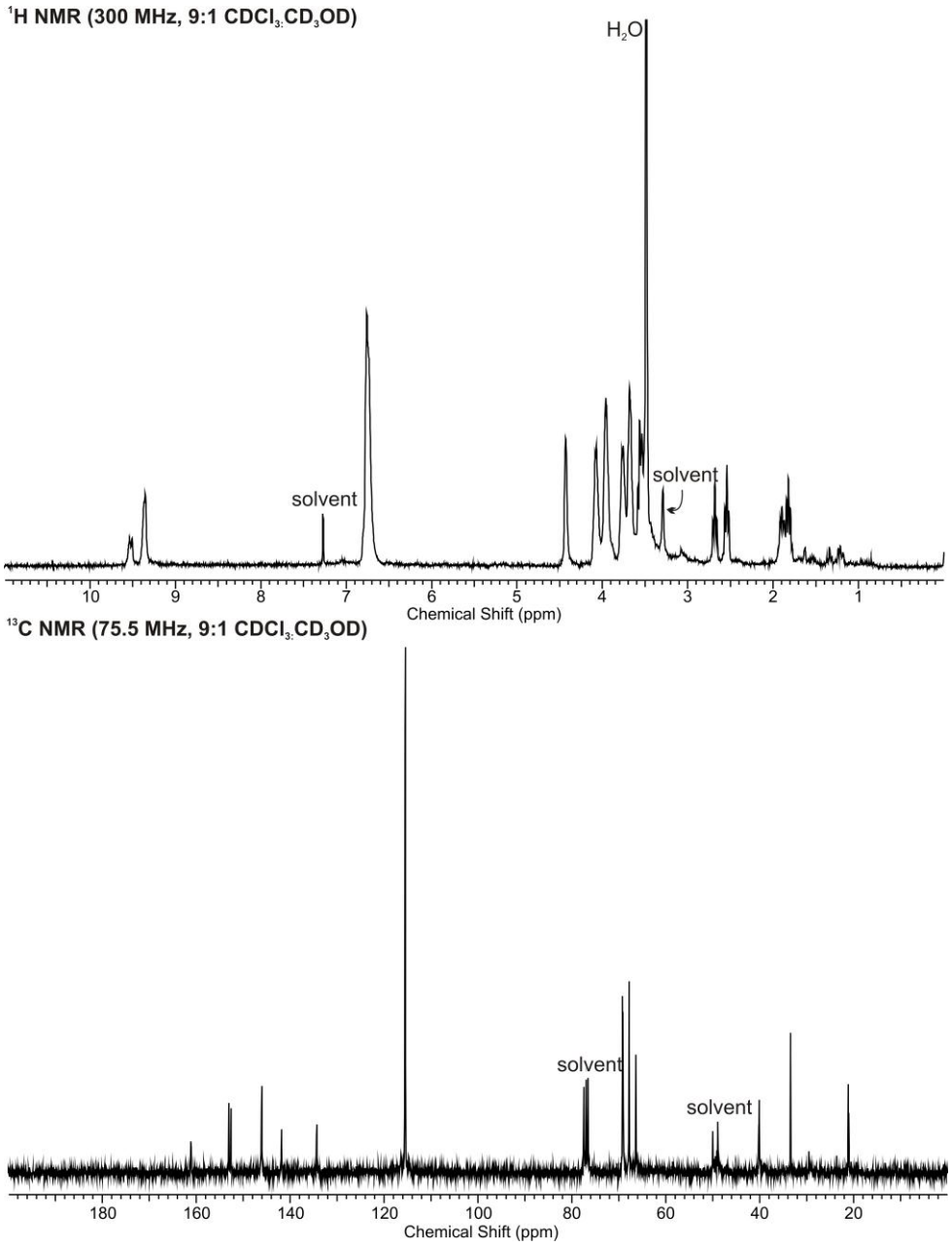

Supplementary Figure 14: ^{1}H and ^{13}C NMR spectra of bis-thiol **5**.Cl.

4) Further crystallographic information

General Methods

Single crystal X-ray diffraction data were collected either using graphite monochromated Mo Kα radiation (λ = 0.71073 Å) on a Nonius KappaCCD diffractometer (for large and well diffracting crystals), mirror monochromated Cu Kα radiation (λ = 1.54180 Å) on an Oxford Diffraction Dual Source SuperNova diffractometer (for smaller crystals), or (for very small or weakly diffracting crystals) using silicon double crystal monochromated synchrotron radiation (λ = 0.68890 Å) at Diamond Light Source beamline I19 on a custom built Rigaku diffractometer. All diffractometers were equipped with a Cryostream N_2 open-flow cooling device.[6] Cell parameters, integration, and scaling were performed using the DENZO-SMN package[7] on the Nonius machine, CrysAlisPro[8] on the Oxford Diffraction instrument, or CrystalClear[9] for synchrotron data.

The structures were solved by direct methods using the SIR92[10] software or by charge flipping using SuperFlip.[11] The structures were refined using full-matrix least-squares on F^2 within the CRYSTALS suite.[12] All non-hydrogen atoms were refined with anisotropic displacement parameters, unless specified otherwise. Disordered portions were modelled using refined partial occupancies. Geometric and vibrational restraints were applied where appropriate to ensure physically reasonable models. The H atoms were usually located in the difference map, but those attached to carbon atoms were repositioned geometrically. Protic H atoms which could not be located in the difference map were positioned to satisfy hydrogen bonding requirements. The H atoms were initially refined with soft restraints on the bond lengths and angles to regularize their geometry, after which the positions were refined with riding constraints.

Thermal ellipsoid images and additional notes (including actual crystal data parameters in the case of macrocycle **1**) for each structure are given below.

Macrocycle **1**

Crystals were grown by the slow evaporation of a dichloromethane solution of **1** and diffraction data were collected using synchrotron radiation. The sample diffracted very weakly, and at high angles the reflections were completely absent, even when subjected to synchrotron radiation. After partial structure solution using SuperFlip, the remainder of the molecule was assembled using cycles of Fourier refinement, and a portion of the solvent required use of PLATON SQUEEZE.[13] Despite the low resolution of the diffraction data, the connectivity and gross conformation are not in doubt.

Crystal data. $C_{42}H_{46}FeN_2O_9$, M = 778.68, monoclinic, a = 13.831(6) Å, b = 16.175(7) Å, c = 18.572(9) Å, α = 90°, β = 111.60(6)°, γ = 90°, V = 3863(3) Å^3, T = 150(2) K, space group $P2_1/c$, Z = 4. 2 325 reflections measured, 2 349 were independent (R_{int} = 0.174); final R = 0.0841 (I > 2σ(I)) and wR = 0.1624 (I > 2σ(I)), final R = 0.1588 (all data) and wR = 0.2217 (all data); GOF on F^2 = 1.0844.

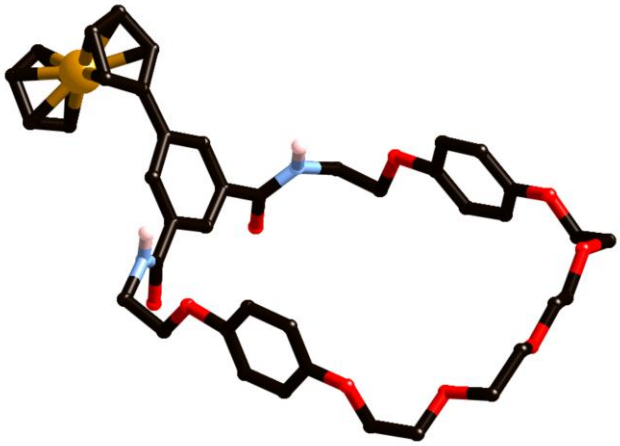

Supplementary Figure 15: Crystal structure of macrocycle **1**.

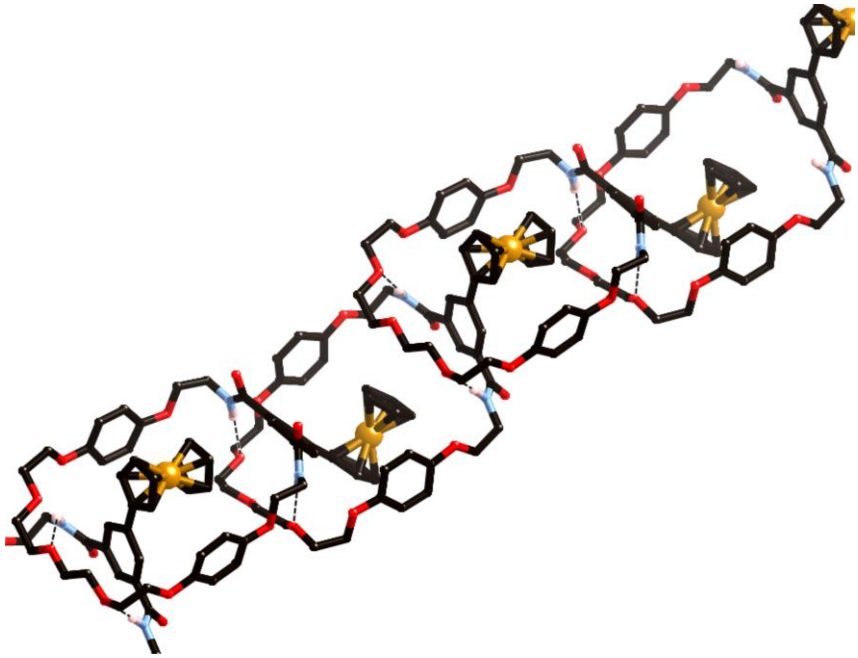

Supplementary Figure 16: Crystal structure of macrocycle **1**, illustrating daisy-chain like packing of macrocycles in the crystal.

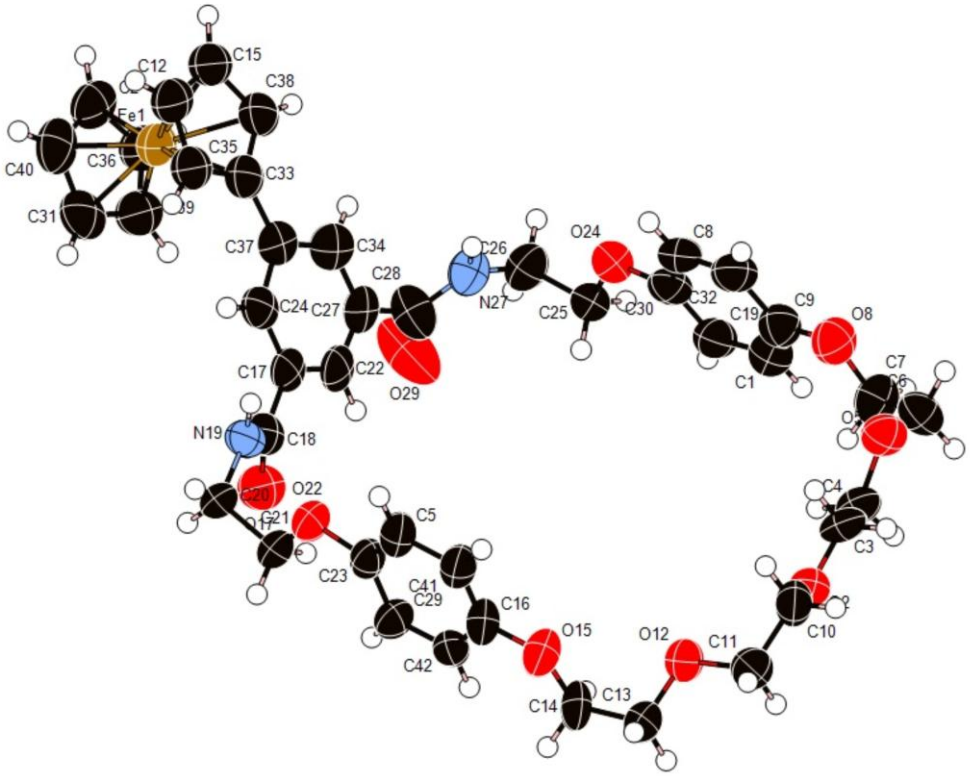

Supplementary Figure 17: Thermal ellipsoid image of crystal structure of macrocycle **1**. Ellipsoids set at 50% probability.

[2]Catenane **3**.Cl

Single crystals of [2]catenane **3**.Cl were grown by the evaporation of an acetonitrile/chloroform solution, which were small and poorly diffracting, and data were collected using synchrotron radiation. Several attempts demonstrated that the crystals suffered severe radiation damage, resulting in a shortage of data. Copious restraints (obtained using Mogul analysis) were necessary to try to ensure that the refinement remained stable and maintained sensible geometric parameters. Modelling the solvent was extremely problematic and PLATON SQUEEZE[13] was therefore used to account for this portion.

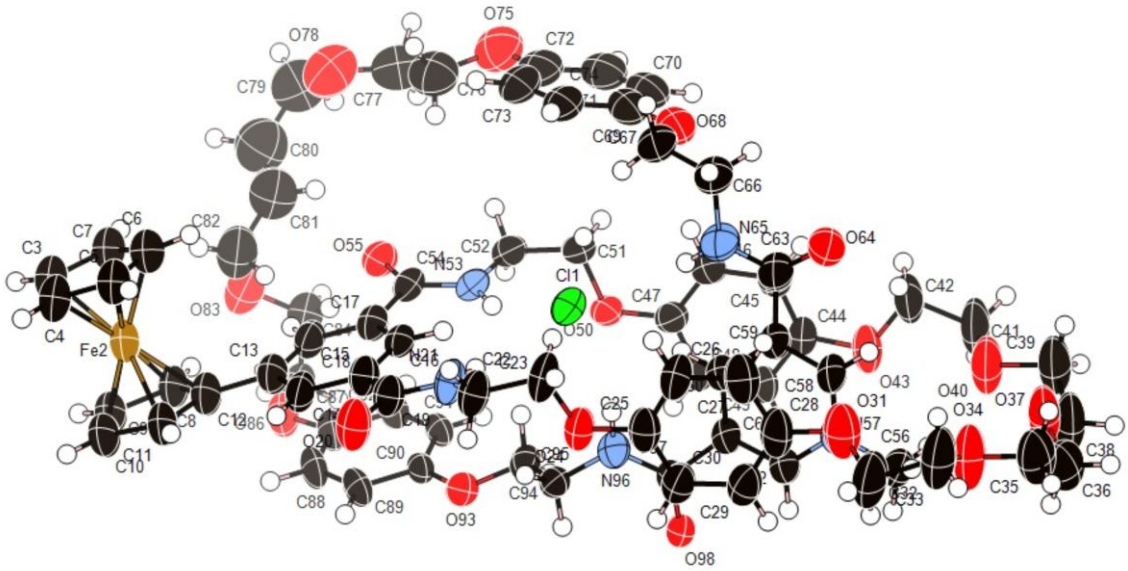

Supplementary Figure 18: Thermal ellipsoid image of crystal structure of [2]catenane **3**.Cl. Ellipsoids set at 25% probability.

[3]Catenane **4**.$(Cl)_2$

Single crystals of [3]catenane **4**.$(Cl)_2$ were grown by slow diffusion of diisopropyl ether into a chloroform solution. Diffraction data were collected using Cu Kα radiation. The disordered chloroform molecules and polyether chains were modelled using refined partial occupancies over two sites for each segment. Although this generally produced a satisfactory model, a third component of disorder in the polyether portion was suggested by the residual electron density. However, no meaningful model could be constructed to account for this. Due to this additional disorder, the refinement would not converge until rigid body refinement was used for the polyether chains.

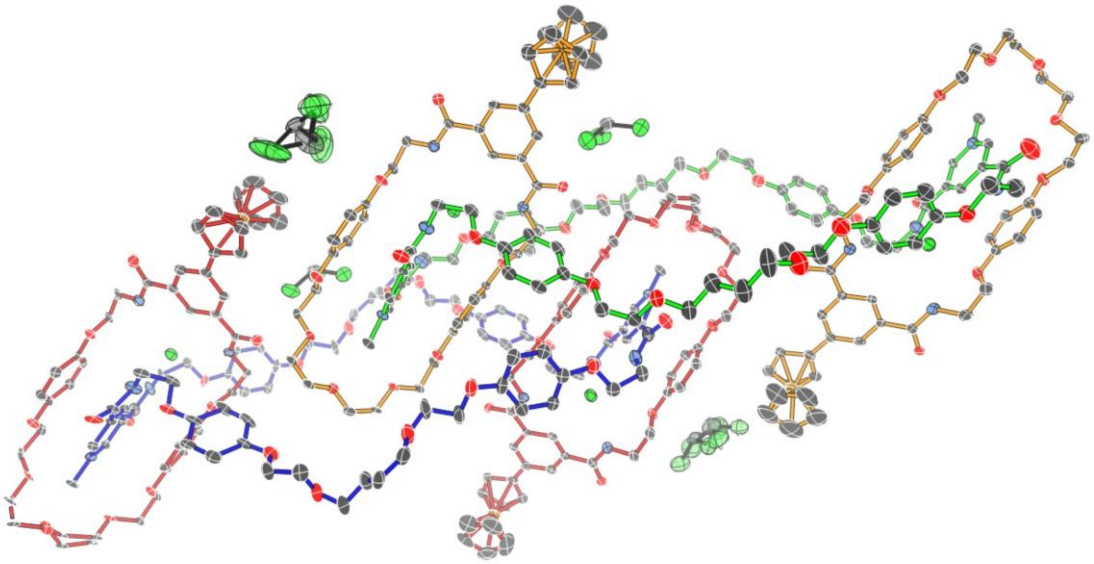

Supplementary Figure 19: Thermal ellipsoid image of crystal structure of [3]catenane **4**.$(Cl)_2$. Ellipsoids set at 50% probability. Hydrogen atoms omitted for clarity. The two crystallographically independent [3]catenanes are designated by colored bonds – a red/blue and an orange/green assembly respectively.

Pseudorotaxane **1**.**5**.Cl

Single crystals of pseudorotaxane **1**.**5**.Cl were grown by slow evaporation of a dichloromethane solution of **1** and **5**.Cl. Data were collected using synchrotron radiation. The crystals diffracted extremely poorly, displaying a high mosaic spread and reaching a resolution limit of ca. 1.5 Å. Series of ω-scans were performed in such a way as to cover a sphere of data to a maximum resolution of 0.90 Å. Significant restraints were applied (with the aid of MOGUL) to correct unreasonable geometries.

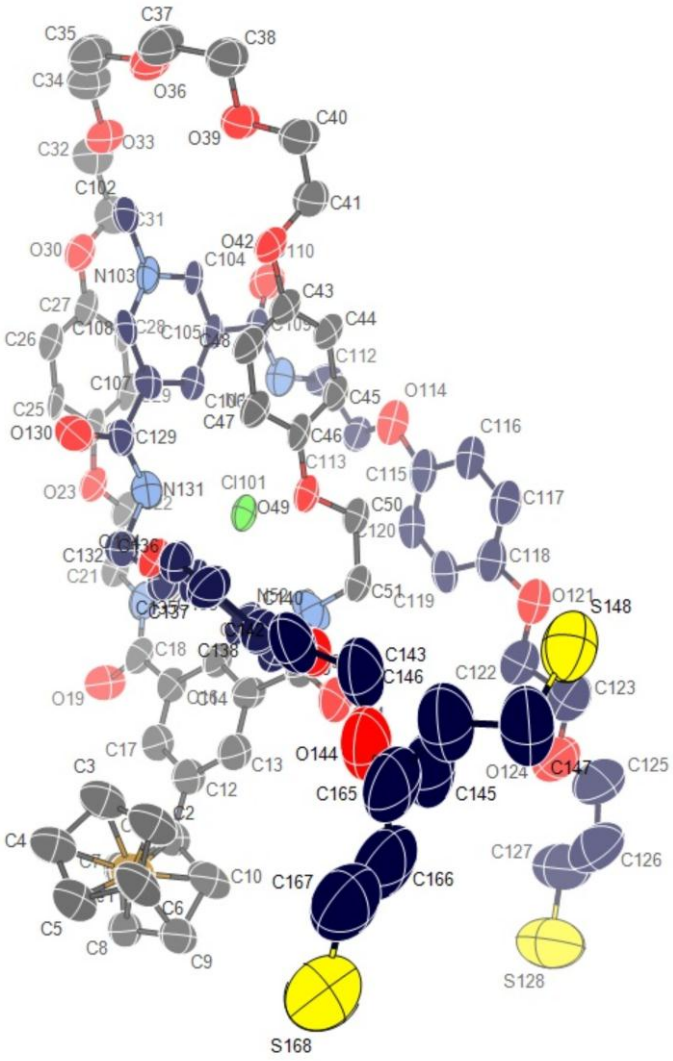

Supplementary Figure 20: Thermal ellipsoid image of crystal structure of pseudorotaxane **9**.**16**.Cl. Ellipsoids set at 25% probability. Hydrogen atoms omitted for clarity.

4) Anion recognition studies of solution phase species

^{1}H NMR titrations

Protocol

^{1}H NMR spectra were recorded on a Varian Unity Plus 500 spectrometer. In a typical experiment, a solution of guest was added to a solution of the host (either macrocycle **1** or [2]catenane **3**.PF_6) at 293 K. The chemical shift of specific proton(s) was monitored for seventeen titration points (for 0, 0.2, 0.4, 0.6, 0.8, 1.0, 1.2, 1.4, 1.6, 1.8, 2.0, 2.5, 3.0, 4.0, 5.0, 7.0 and 10.0 equivalents of added guest), with the resulting data analysed using the WinEqNMR2 computer program[14], as the association of guest and host was found to be fast on the NMR timescale for all systems.

The anion binding titration experiments were carried out using salts of the non-complexing tetrabutylammonium (TBA) cation as the guest species, titrated into the dissolved host. A 0.075 M solution of anion was added to 0.50 mL of a 1.50 mM solution of host, i.e. 10 μL is 1 equivalent. The volumes of TBA salt added were 10 x 2 μL, 2 x 5 μL, 2 x 10 μL, 1 x 20 μL and 1 x 30 μL.

The values of the observed chemical shift and the guest concentration were entered into winEQNMR2 for every titration point and, estimates for the binding constant and limiting chemical shifts were made. The parameters were refined using non-linear squares analysis to obtain the best fit between observed and calculated chemical shifts for a 1:1 binding stoichiometry. The program plots the observed chemical shift versus the guest concentration, revealing the accuracy of the experimental data and the suitability of the model used. The input parameters were varied until the best-fit values of the stability constants, and their errors, converged.

Electrochemical titrations

Protocol

Cyclic voltammetry (CV) and square wave voltammetry (SWV) were performed on an Autolab Potentiostat/Galvanostat model PG-STAT 12, controlled by General Purpose Electrochemical System Software v. 4.9 (Eco Chemie). A standard one-compartment three-electrode electrochemical cell, located inside a Faraday cage, was used with a glassy carbon solid disc working electrode, a platinum wire auxiliary electrode and an Innovative Instruments, Inc. LF-2 leak-free silver/silver chloride reference electrode. A 0.5 mM ferrocene sample was used to check the reference electrode and internal resistance of the equipment. The electrolyte solution used in all experiments was 0.1 M $TBAPF_6$ in MeCN.

CVs were typically recorded with a 1 s equilibration time, a step potential of 1 mV and a scan rate of 100 mVs^{-1}. SWVs were typically recorded with a 1 s equilibration time, a step potential of 3 mV and a frequency of 30 Hz. The working electrode was cleaned between scans by polishing with commercially available microcloth.

In a typical experiment, the host (0.5 mM) was dissolved in 2.5 mL of a solution of $TBAPF_6$ (0.1 M) and cyclic and square wave voltammograms were recorded. For the cyclic voltammetry scan rates of 25, 50, 75, 100, 250 and 500 mVs^{-1} were used to test for reversibility. Anion binding experiments were performed by addition of 0, 0.5, 1, 2 and 5 equivalents of anion (as a 0.25 M solution of TBAX salt in electrolyte solution, 5 µL is 1 equivalent) to a 2.5 mL aliquot of the receptor solution, stirred and the cyclic and square wave voltammograms recorded.

Electrochemical data

I. Reversibility

For an electrochemical system (under fast kinetics) to be described as reversible, the following criteria must be satisfied:

(i) ΔE = 59/n mV (where n = number of electrons transferred in the redox process), so here where n = 1, ΔE should equal 59 mV;

(ii) E_{pa} and E_{pc} are independent of the scan rate;

(iii) I_{pa} / I_{pc} = 1;

(iv) I_{pa} and I_{pc} are proportional to the square root of the scan rate.

From CVs of macrocycle **1** and catenane **3**.PF_6 recorded at varying scan rates, it is best to describe macrocycle **1** and catenane **3**.PF_6 as being quasi-reversible electrochemical systems because the data almost fit the outlined criteria.

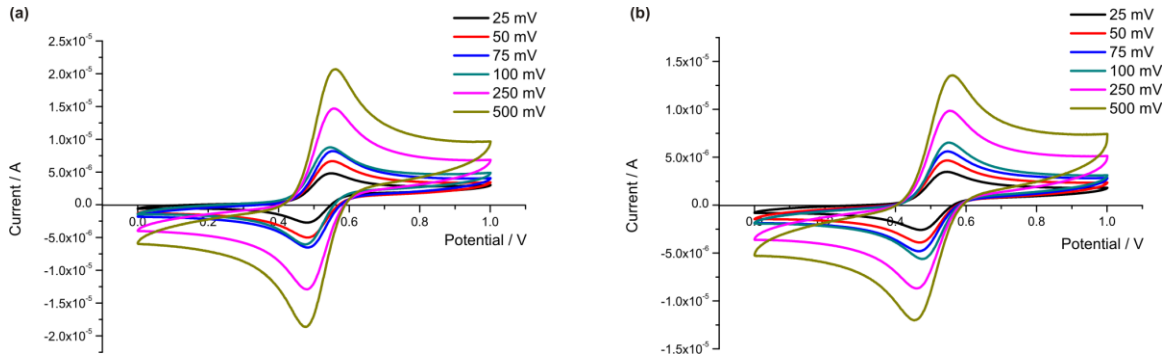

Supplementary Fig. 21: CVs of (a) Macrocycle **1** and (b) Catenane **3**.PF_6 in 0.1 M $TBAPF_6/CH_3CN:CH_2Cl_2$ (1:1), with varying scan rates (Potential compared to a Ag/AgCl reference).

Supp. Table 1 ΔE, E_{pa}, E_{pc} and I_{pa}/I_{pc} data for macrocycle **1** and catenane **3**.PF_6 for various scan rates[a]

Scan Rate / mV	Macrocycle **1**				Catenane **3**.PF_6			
	ΔE / V	E_{pa} / V	E_{pc} / V	I_{pa}/I_{pc}	ΔE / V	E_{pa} / V	E_{pc} / V	I_{pa}/I_{pc}
25	0.064	0.547	0.483	1.03	0.073	0.546	0.473	1.05
50	0.068	0.551	0.483	1.03	0.075	0.546	0.471	1.04
75	0.069	0.553	0.484	1.06	0.080	0.548	0.468	1.05
100	0.070	0.547	0.477	1.02	0.071	0.550	0.479	1.05
250	0.073	0.554	0.481	1.04	0.091	0.552	0.461	1.09
500	0.081	0.560	0.479	1.02	0.106	0.559	0.453	1.09

[a] Electrolyte: 0.1 M $TBAPF_6/CH_3CN:CH_2Cl_2$ (1:1). Potential compared to a Ag/AgCl reference.

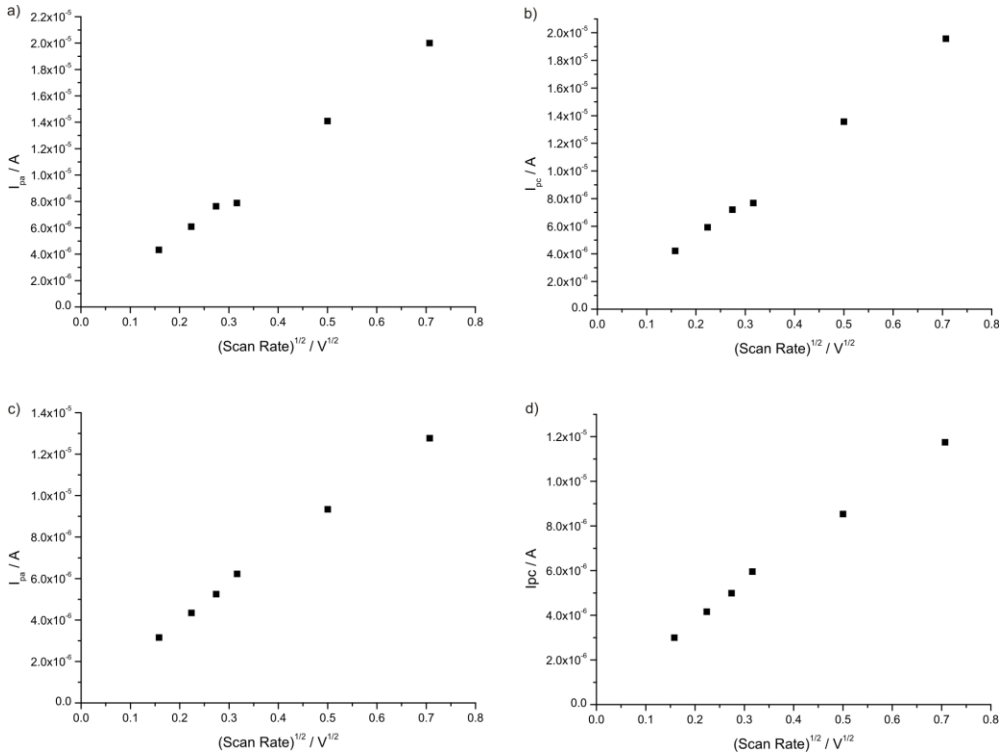

Supplementary Fig. 22**:** Plots of I_{pa} and I_{pc} against (scan rate)$^{1/2}$ for macrocycle **1** [(a) and (b)] and catenane **3**.PF_6 [(c) and (d)].

II. CVs of anion titration experiments

Macrocycle **1** ($E_{1/2}$ = + 80 mV relative to $E_{1/2(ferrocene)}$ = 0 V)

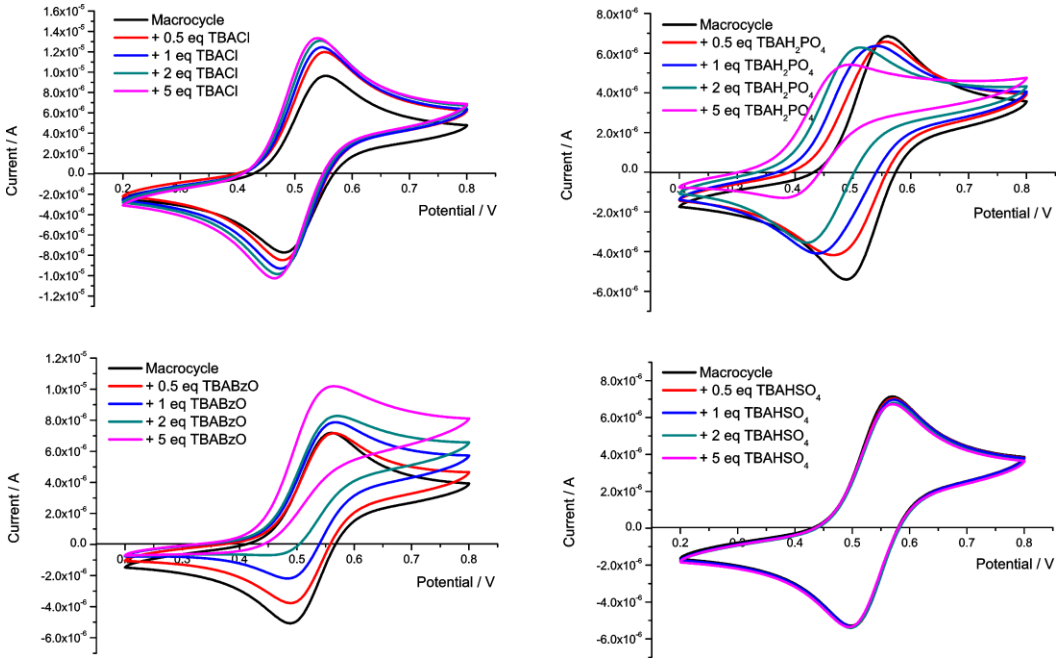

Supplementary Fig. 23**:** CVs of macrocycle **1** in 0.1 M $TBAPF_6$/1:1 CH_2Cl_2/CH_3CN upon the addition of aliquots of various anions (added as TBA salts). Potential compared to Ag/AgCl.

Catenane **3**.PF_6 ($E_{1/2}$ = + 75 mV relative to $E_{1/2(ferrocene)}$ = 0 V)

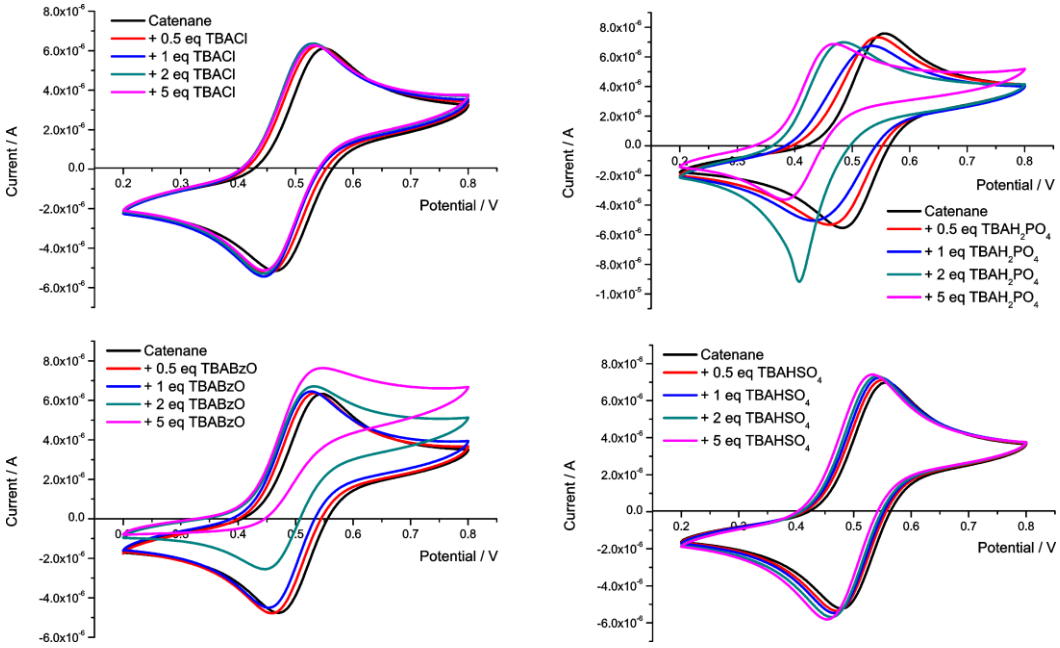

Supplementary Fig. 24**:** CVs of catenane **3**.PF_6 in 0.1 M $TBAPF_6$/1:1 CH_2Cl_2/CH_3CN upon the addition of aliquots of various anions (added as TBA salts). Potential compared to Ag/AgCl.

III SWs of anion titration experiments

Macrocycle **1**

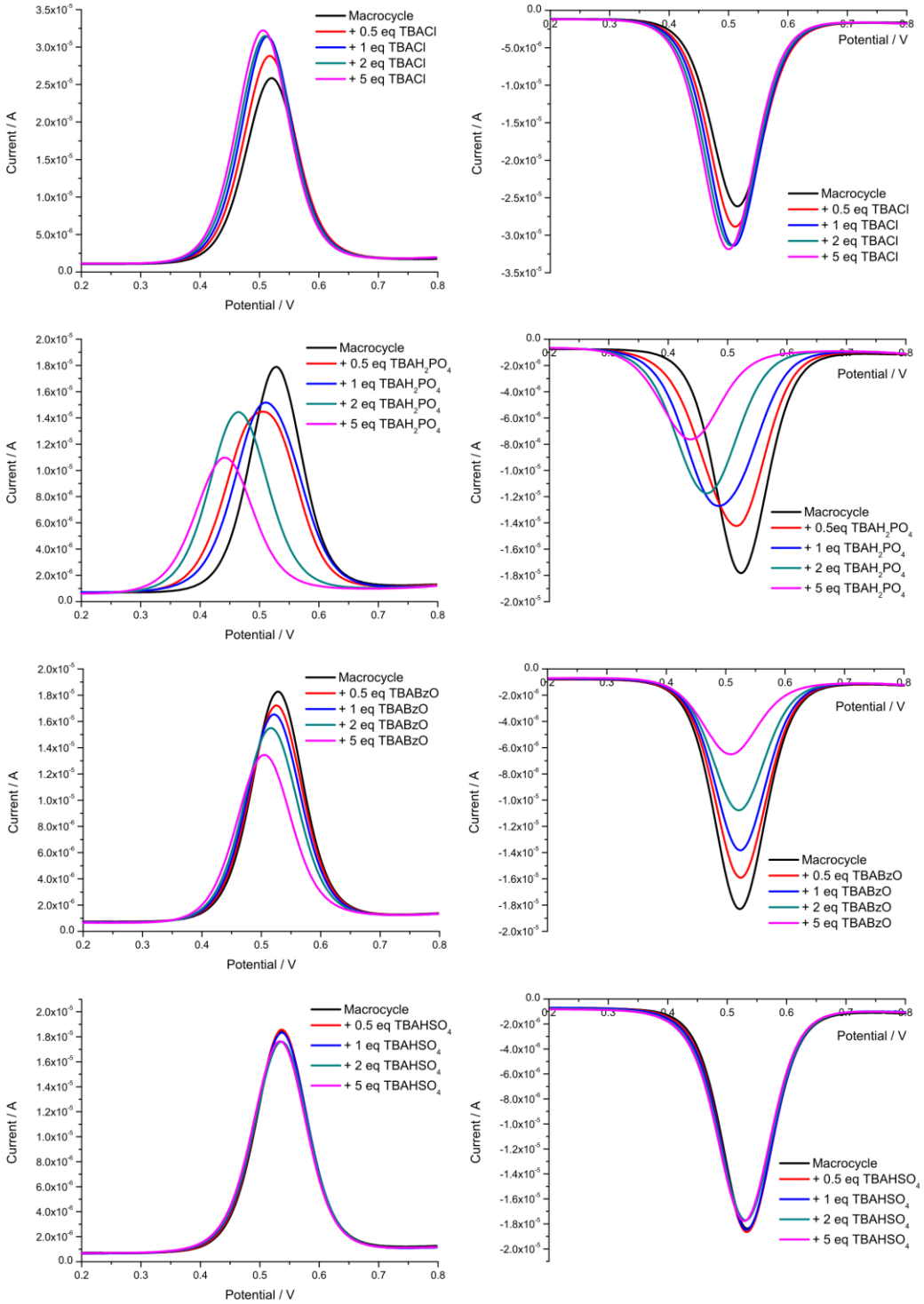

Supplementary Fig. 25**:** SWVs of macrocycle **1** in 0.1 M $TBAPF_6$/1:1 CH_2Cl_2/CH_3CN upon the addition of aliquots of various anions (added as TBA salts). Potential compared to Ag/AgCl.

Catenane **3**.PF_6

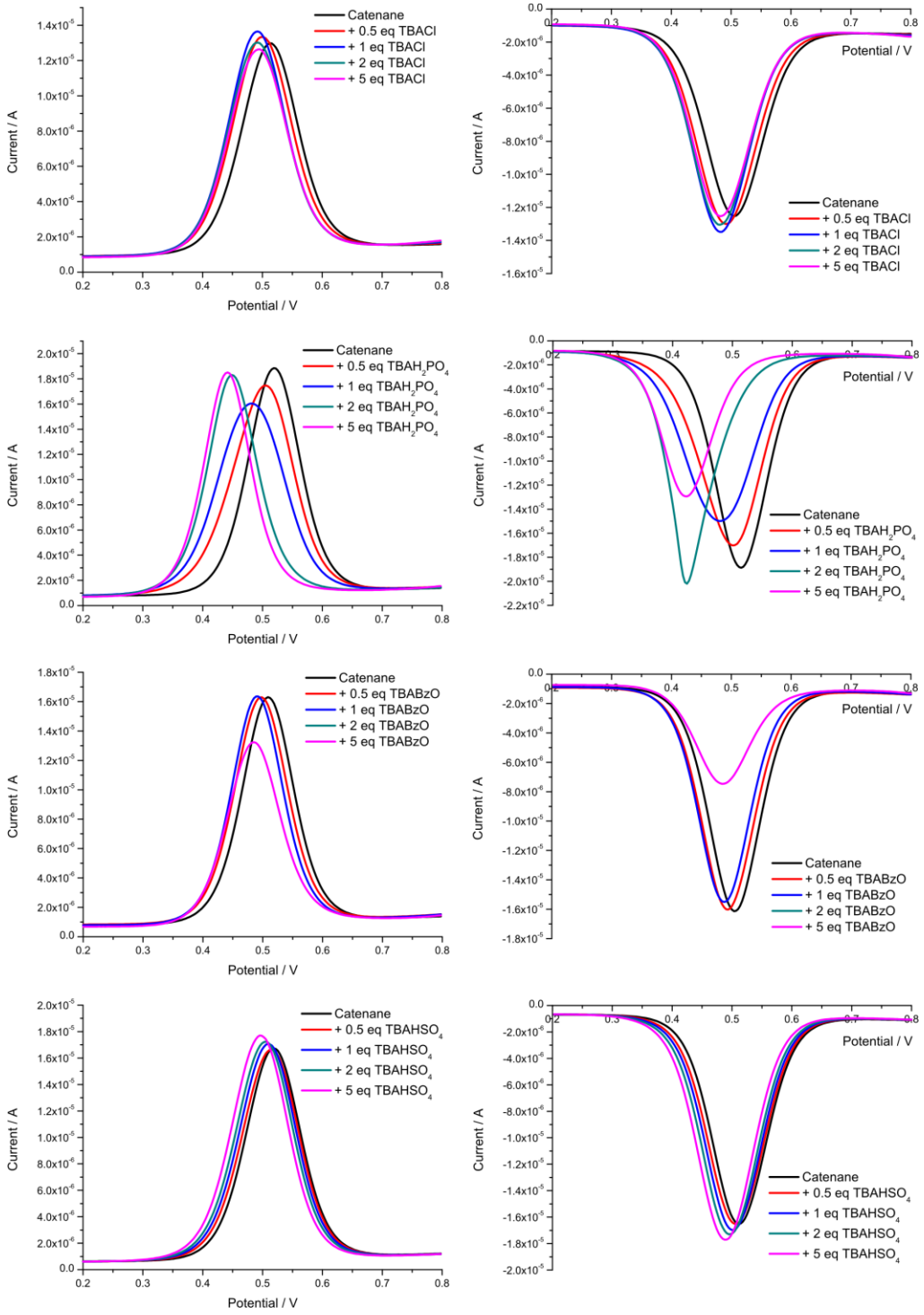

Supplementary Fig. 26: SWVs of catenane **3**.PF_6 in 0.1 M $TBAPF_6$/1:1 CH_2Cl_2/CH_3CN upon the addition of aliquots of various anions (added as TBA salts). Potential compared to Ag/AgCl.

5) Formation and characterization of catenane SAMs

I) General Methods

Monolayer formation

Gold working electrodes were employed (1 mm diameter, Bioanalytical Systems, *BAS*). Prior to SAM formation these were treated with hot piranha solution (70% H_2SO_4:30% H_2O_2) followed by mechanical polishing to a mirror finish using aluminium oxide disks (Buehler, Fibrmet Discs) with polishing progressing from coarse (3 μm) to fine (0.3 μm). *CAUTION: Piranha solution can react violently with organic materials, and should be handled with extreme caution! Piranha solution should not be stored in tightly sealed containers.* This was followed by electrochemical polishing in 0.5 M sulfuric acid and potential scanning between -0.5 V to ca. 1.3 V vs a Ag/AgCl reference electrode at a sweep rate of 100 mV s^{-1}.[15] Electrodes were finished by cycling in the negative potential range (–0.5 to –1 V vs Ag/AgCl) then used immediately for SAM formation. The active Au electrode surface area was determined from the charge of the gold oxide monolayer reduction peak and converted the real surface area using a conversion factor of 482 μC cm^{-2}.[16] Pristine electropolished gold electrodes were then exposed to a 1 mM solution containing ten equivalents of macrocycle **1** with respect to the pyridinium threading component **5.**Cl in CH_2Cl_2 for 8 h, resulting in the formation of the surface chemisorbed catenane. After the given immersion time, the modified electrodes were removed from its proprietary solutions and washed thoroughly with CH_2Cl_2 and CH_3CN to remove any adventitious physisorbed material from the surface. The modified electrodes were then transferred to designated electrochemical cells containing deaerated solvents containing 0.1 M supporting electrolyte.

Electrochemical studies

Electrochemical investigations on SAM modified gold electrodes were performed on an Autolab PGSTAT12 running GPES software (General Purpose Electrochemical System – Version 4.9, Eco Chemie) equipped with SCANGEN and ADC750 (analogue-digital converter) modules for fast scan rates (> 10 V s^{-1}) and an ECD (electrochemical detection) module to improve current sensitivity at slower scan rates (< 1 V s^{-1}). Uncompensated resistance was minimized using the built-in positive-feedback iR compensation feature. All electrochemistry was carried out in a standard three-electrode setup. All potentials are referenced to a Ag/AgCl ("no leak" Cypress system reference electrode). Platinum gauze was employed as the counter electrode.

Ellipsometry

Ellipsometry measurements were performed using a Picometer Ellipsometer (Beaglehole Instruments, Wellington, New Zealand) with a refractive index of 1.45 for the monolayer over the gold layer (with pseudo optical constants of $n + ik = 0.7699 + i \times 3.7439$ determined from a fit to a bare gold substrate. The

Au substrates for use in ellipsometry measurements were prepared by evaporative coating of cleaned Si(100) wafers (Si-Mat) with a 2 nm Cr (RD Mathis) adhesion layer, followed by a 15 nm layer of Au (Alfa Aesar, 99.99%).

X-ray photoelectron spectroscopy

Gold substrates for use in X-ray photoelectron spectroscopy (XPS) analysis were prepared by evaporative coating of cleaned Si(100) wafers (Si-Tech, p-doped, nominal resistivity of 5 Ω cm, 0.4 mm thick) with a 2 nm Cr (RD Mathis) adhesion layer, followed by a 30 nm layer of Au (Alfa Aesar, 99.99%). Catenane SAM **1**.**5**.Cl modified Au surfaces were prepared as described above.

High-resolution XPS spectra were collected on a Scienta ESCA 3000 (NCESS, Daresbury, UK)[17] spectrometer employing a high power rotating anode and monochromatised A1Kα radiation (hυ = 1486.7 eV) source with a power of 150 W. The typical operating pressure was below 10^{-8} Torr in the analysis chamber. All spectra were collected using a constant analyzer pass energy of 150 eV, a dwell time of 0.1 s, and a scan step of 0.05 eV. Binding energy corrections were made by referencing all spectra to the Au $4f_{7/2}$ peak at 84.0 eV. Relative atomic concentrations were determined by integrating spectra that were fitted with mixed Gaussian/Lorentzian profile peak shapes after subtraction of a Shirley type background. The atomic sensitivity factors employed in this study for comparison of relative heteroatomic concentrations were obtained from an online library and are as follows: $S_{C\ 1s}$: 0.25, $S_{S\ 2p}$: 0.54, $S_{O\ 1s}$: 0.66, $S_{N\ 1s}$: 0.42, $S_{Fe\ 2p}$: 2.0, $S_{Cl\ 2p}$: 0.73 and $S_{Au\ 4f}$: 2.8.[18] All spectra were analyzed and peak-fitted using CasaXPS 2.3.12 software (Casa Software Ltd., Teignmouth, UK). X-ray-induced damage of the monolayer films was negligible under these operating procedures**.**

II) Catenane SAM characterization

Catenane surface concentration

Reductive desorption of catenane SAM **1**.**5**.Cl.Au was performed in aqueous 0.5 M KOH solution to estimate the amount of the thiolate on the electrode surface. The reductive desorption is known to be a one-electron process, and therefore, the amount of adsorbed thiol can be determined straightforwardly from the desorption charge. The appearance of an irreversible peak at –1.2 V vs. Ag/AgCl was attributed to reductive desorption of the monolayer thiol group from the gold surface.[19]

A comparative assessment of macrocycle **1** (through integrated charge from the appended ferrocene) and pyridinium thread (through integrated charge associated with reductive surface stripping) surface coverage, produced a molar ratio close to 1:3, indicative of a significant component of chemisorbed **5**.Cl.Au within the films.

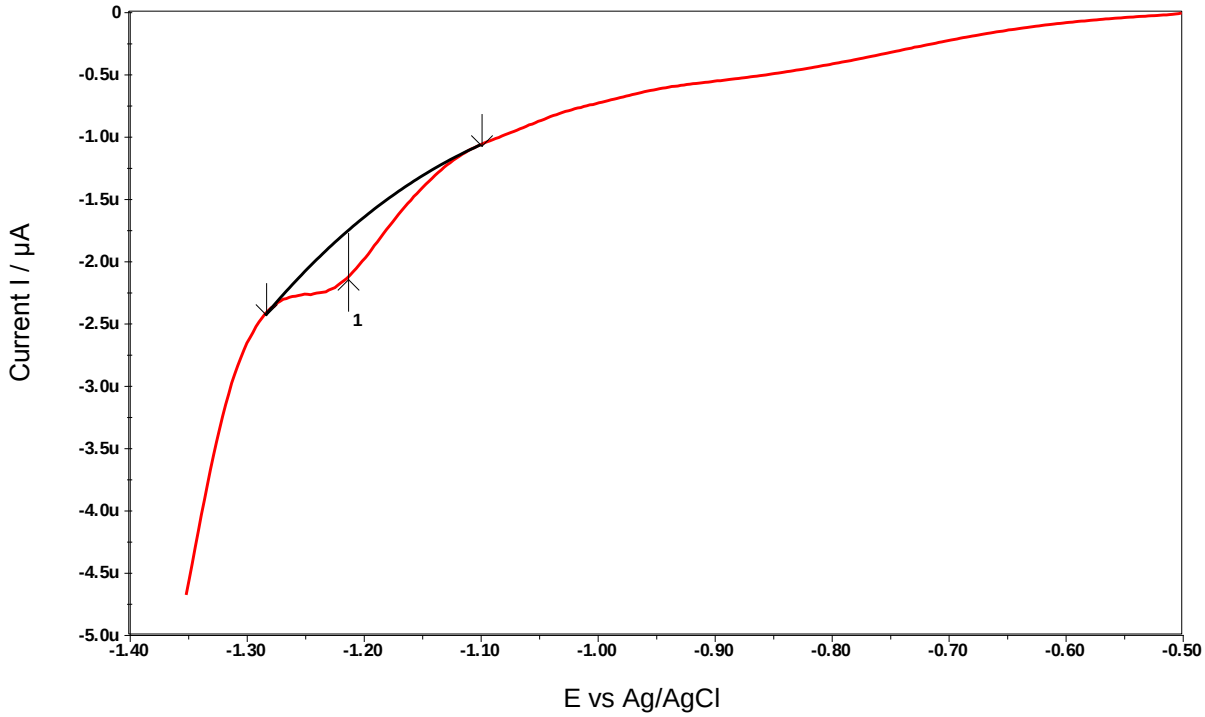

Supplementary Figure 27: Linear sweep voltammogram of catenane SAM **1.5**.Cl.Au in 0.5 M $KOH_{(aq)}$. Scan rate 0.1 V s^{-1}. The irreversible peak at –1.2 V vs Ag/AgCl is of thiol layer reductive stripping.

Kinetic analysis of catenane SAM 1.5. Cl.Au **using Laviron's Formalism**

The electrochemical behaviour of catenane SAM **1.5**.Cl.Au was studied to investigate the effect of the scan rate on the heterogeneous electron-transfer kinetics. A series of well-defined redox peaks were observed and correspond to the electron-transfer process of the interlocked and immobilized ferrocene macrocycle moiety at different scan rates. Anodic and cathodic peak currents increase linearly with scan rate (up to 10 V s^{-1}), which is expected assuming that the ferrocene macrocycle undergoes the quasi-reversible one electron transfer reaction. Anodic and cathodic peak currents were found to be linearly proportional to scan rate from 0.1 V s^{-1} to 10 V s^{-1}, which is consistent with the voltammetric behaviour of a surface confined redox center. Peak potentials shifted with increasing scan rate and peak separation increased, which is characteristic of an immobilized redox species under kinetic control.

The peak potentials are independent of the scan rate at sweep rates < 10 V s^{-1} and proportional to the logarithm of scan rates above 200 V s^{-1}, as predicted by Laviron's theory.

Laviron's formulism was used to evaluate the heterogeneous rate constant *k* for electron transfer in redox-active catenane SAMs.[20]

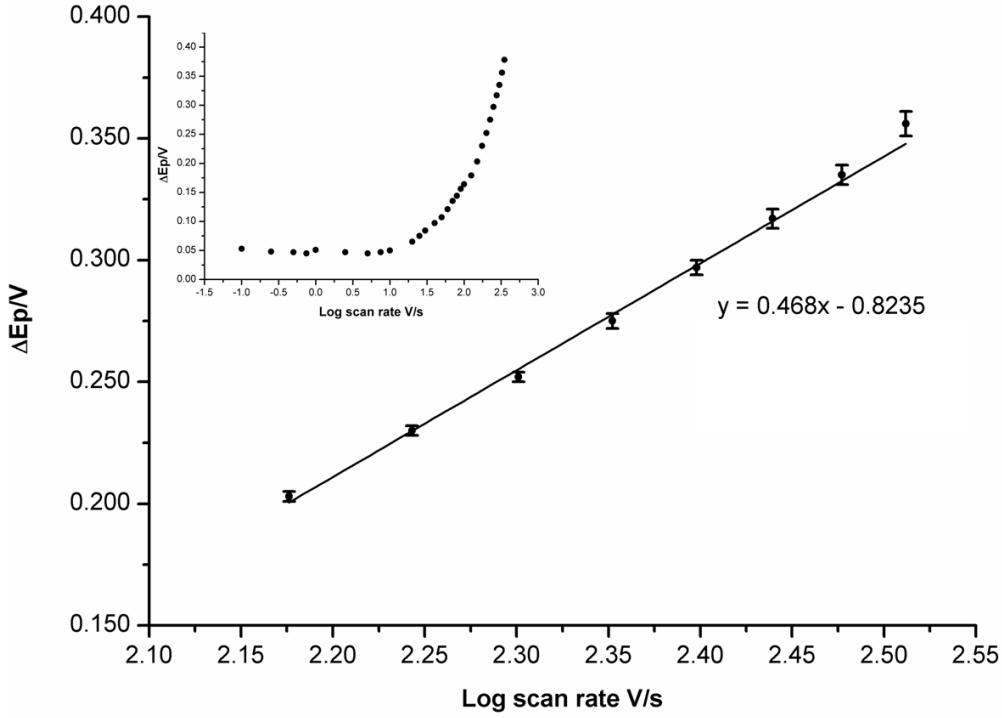

Supplementary Figure 28: Laviron plot for the dependence of peak potentials on logarithm of scan rate of catenane SAM **1.5**.Cl.Au for scan rates above 200 V s^{-1}. Inset shows entire range of scan rates (100 mVs^{-1} to 350 V s^{-1}). Error in peak potential measurement was ca. 3-5mV.

X-Ray photoelectron spectroscopy (XPS)

The self-assembled monolayers **1**.**5**.Cl.Au and **5**.Cl.Au (for comparison) were investigated by X-ray photoelectron spectroscopy (XPS). XPS analyses of Fe 2p, O 1s, N 1s, C 1s, Cl 2p, S 2p and Au 4f regions are provided in Supplementary Figures 29–35. All the elements expected to be present were identified, with particularly unambiguous evidence for the existence of the catenane monolayer being provided by the identification of the Fe $2p_{3/2}$ signal at a binding energy (BE) ~ 708 eV (Supplementary Figure 29), arising from the Fe atom in the ferrocene unit of macrocycle **1**, mechanically bonded to the surface as part of the interlocked structure.

Angle resolved measurements were used to investigate the composition of the catenane SAM **1**.**5**.Cl.Au, by probing several different spectral regions at different measuring angles. Altering the emission angle causes changes in the effective information depth of analysis. At glancing incidence (small angles) only the upper layers of the sample are examined; whereas at higher angles, deeper layers are detected. The number of detected electrons is a measure of the elemental concentration. In order to obtain quantitative results, peak areas were divided by the standard atomic sensitivity factors (and also the inelastic mean free path) to obtain relative atomic concentrations.[21] Supplementary Figures 36 and 37 show the relative concentrations of different elements in the catenane SAM **1**.**5**.Cl.Au, measured at various angles. The lower the concentration ratio the deeper the element is positioned in the monolayer.

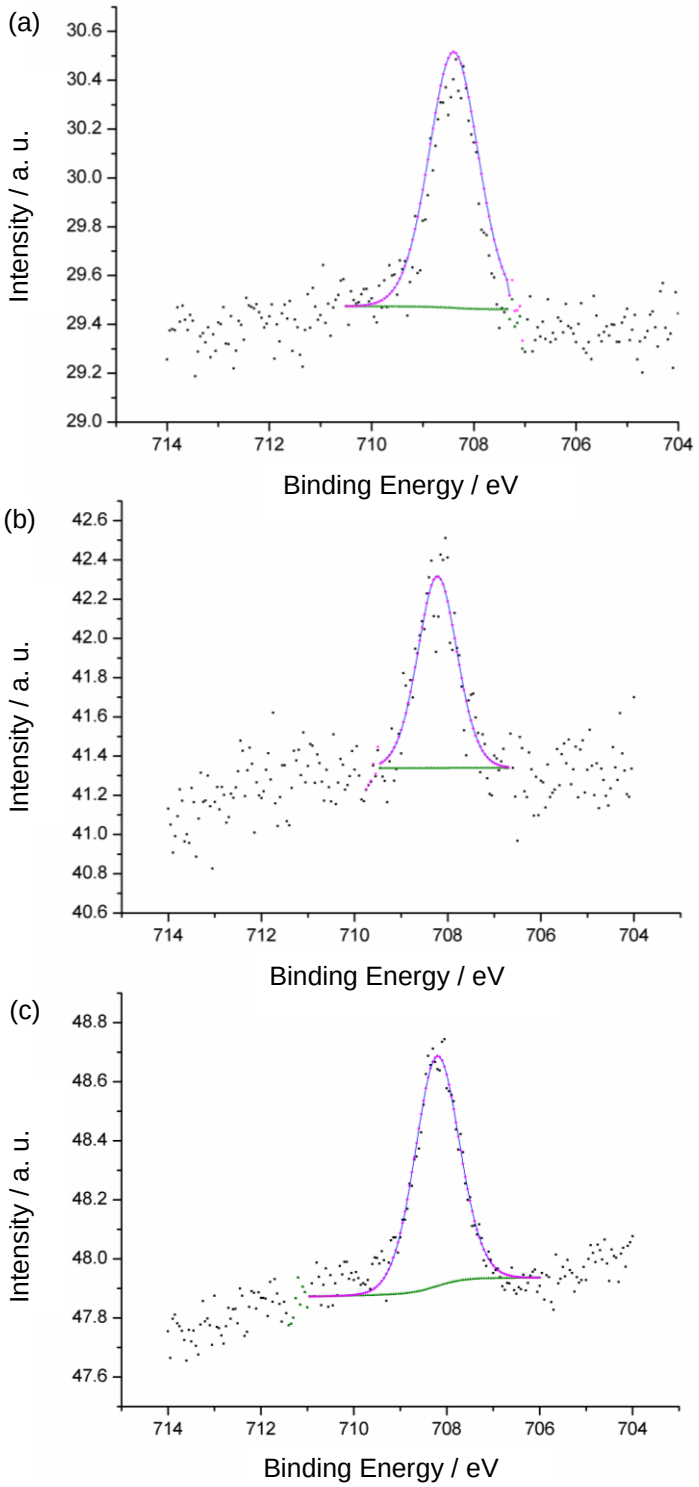

Supplementary Figure 29: The Fe $2p_{3/2}$ high resolution XPS spectra of catenane SAM **1**.**5**.Cl.Au monolayer. XPS spectra acquired at take-off angles (between the sample surface and the energy analyzer**)** of (a): 10°, (b): 40° and (c): 90°. The Fe $2p_{½}$ peak at ~ 720 eV was not resolved. Raw data (●); fit to the experimental data (●); Fe 2p (—●—), and background (●).

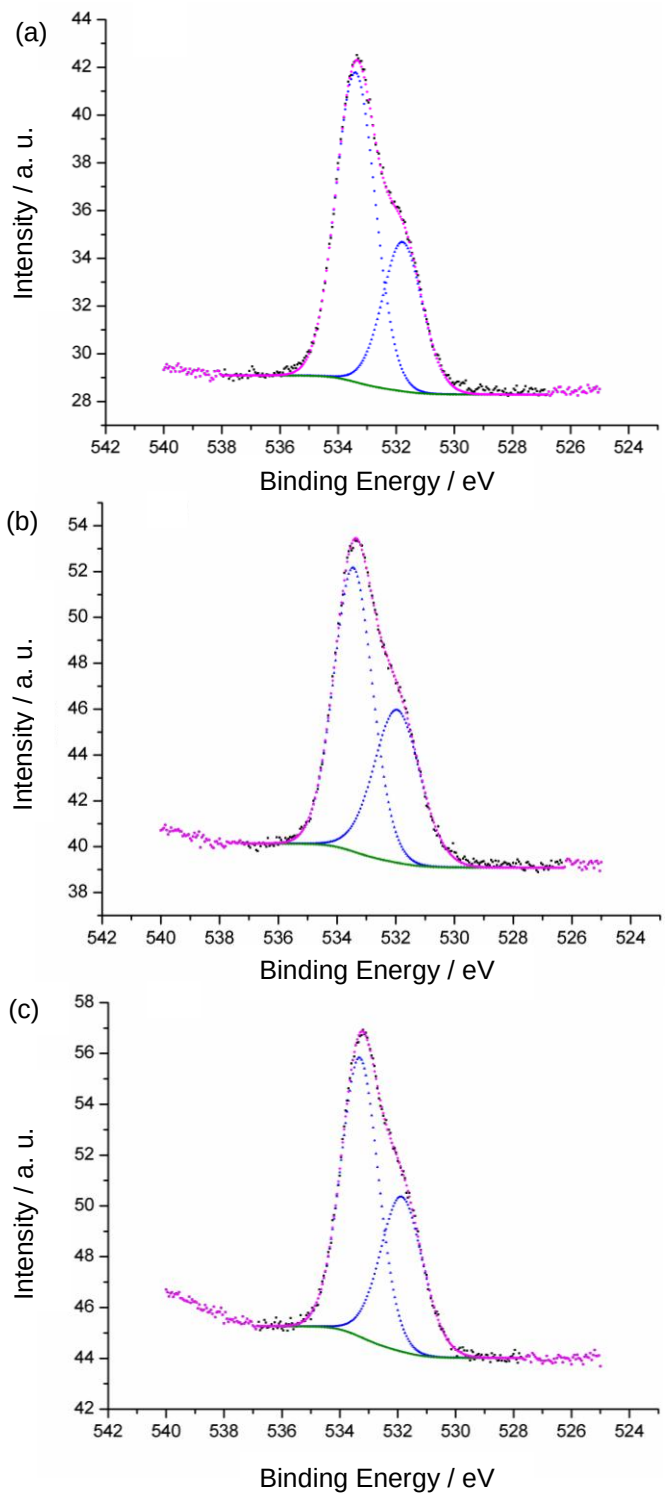

Supplementary Figure 30: The O 1s regions of the high resolution XPS spectra of catenane SAM **1**.**5**.Cl.Au. XPS spectra acquired at take-off angles (between the sample surface and the energy analyzer**)** of (a): 10°, (b): 40° and (c): 90°. Raw data (●); fit to the experimental data (●); O 1s (—●—), and background (●).

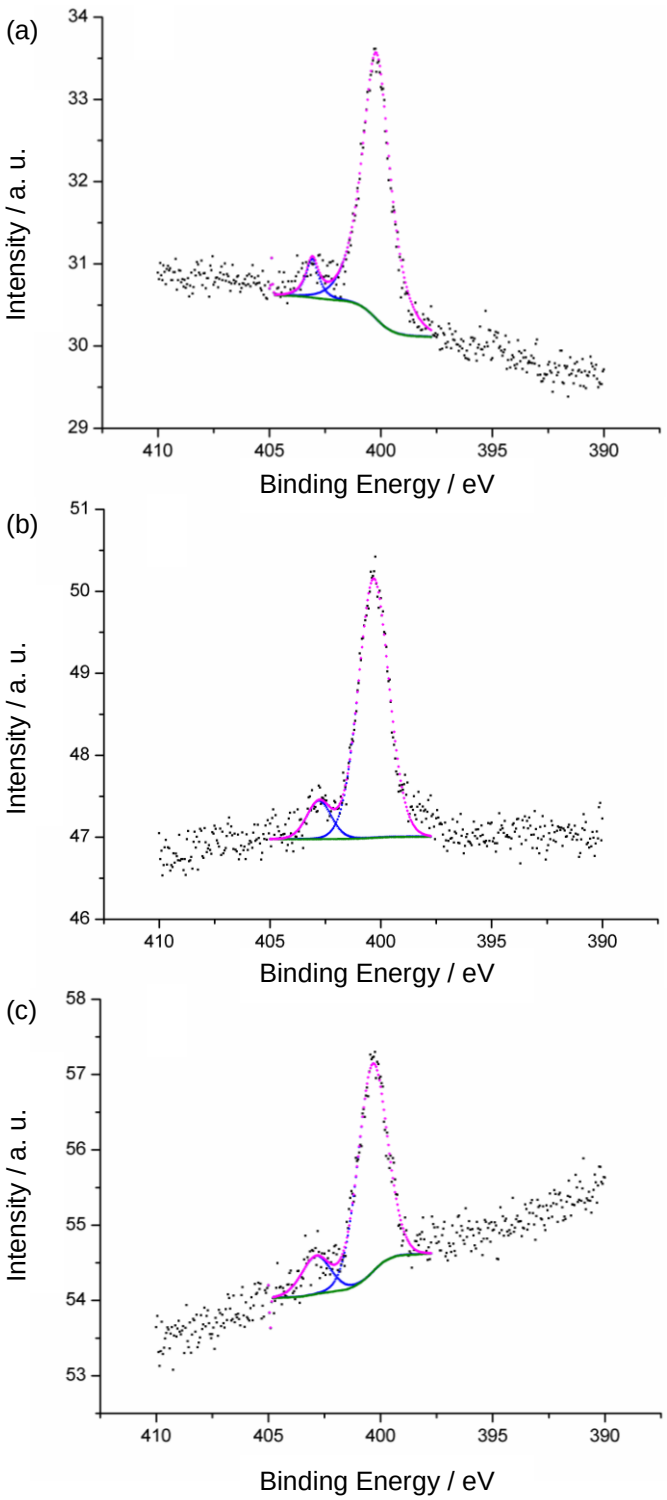

Supplementary Figure 31: The N 1s regions of the high resolution XPS spectra of catenane SAM **1**.**5**.Cl.Au. XPS spectra acquired at take-off angles (between the sample surface and the energy analyzer**)** of (a): 10°, (b): 40° and (c): 90°. Raw data (●); fit to the experimental data (●); N 1s (—●—), and background (●).

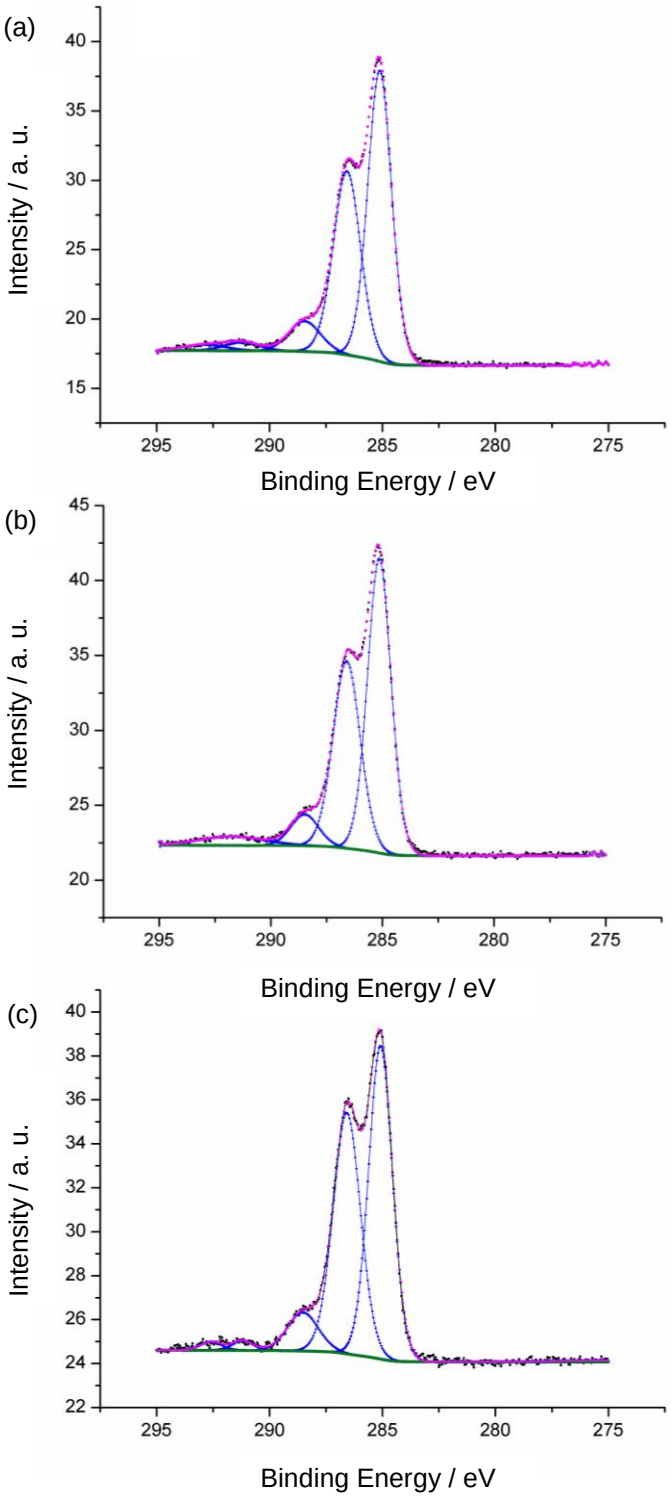

Supplementary Figure 32: The C 1s regions of the high resolution XPS spectra of catenane SAM **1**.**5**.Cl.Au. XPS spectra acquired at take-off angles (between the sample surface and the energy analyzer**)** of (a): 10°, (b): 40° and (c): 90°. Raw data (●); fit to the experimental data (●); C 1s (—●—), and background (●).

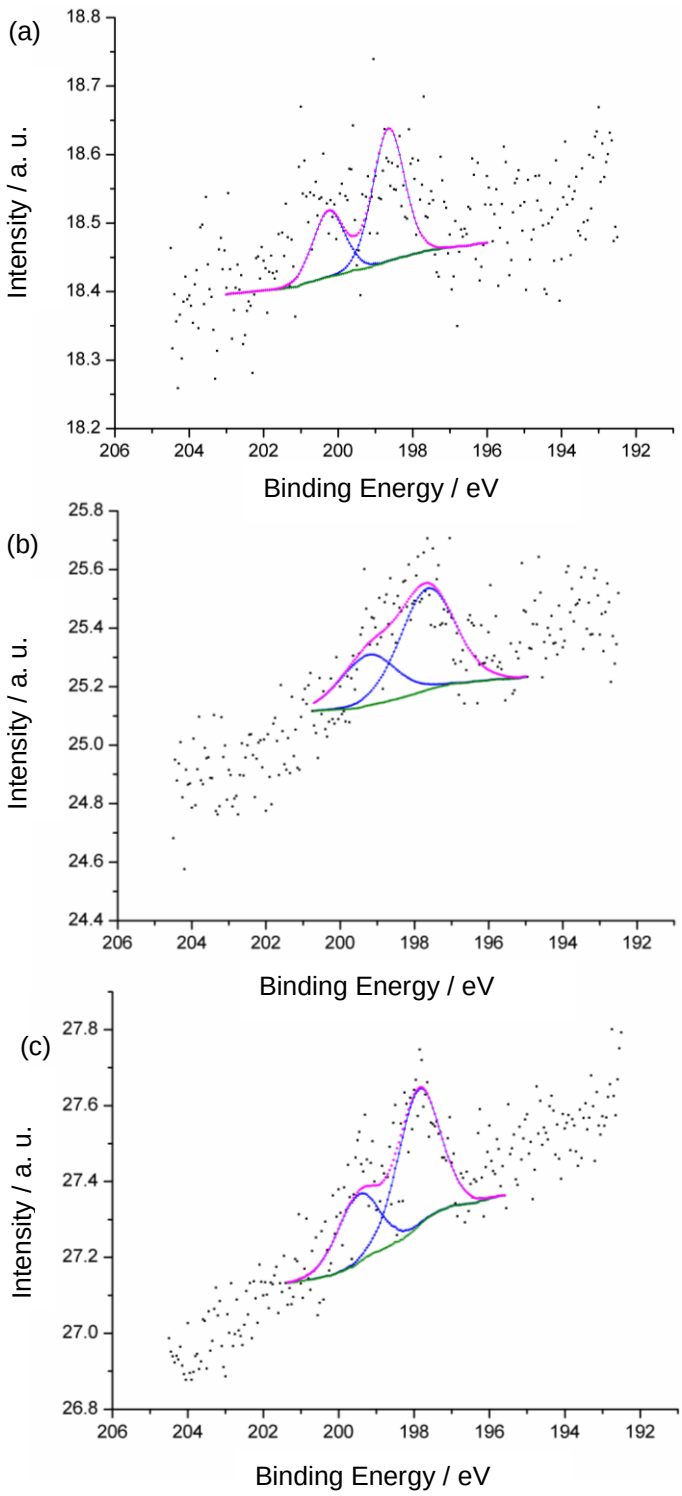

Supplementary Figure 33: The Cl 2p regions of the high resolution XPS spectra of catenane SAM **1.5**.Cl.Au. XPS spectra acquired at take-off angles (between the sample surface and the energy analyzer**)** of (a): 10°, (b): 40° and (c): 90°. Raw data (●); fit to the experimental data (●); Cl 2p (—●—), and background (●). Cl 2p core level spectra were fitted with a single doublet of equal (FWHM), a doublet separation of 1.6 eV, and a Cl $2p_{3/2}$/Cl $2p_{1/2}$ peak area ratio of 2:1.

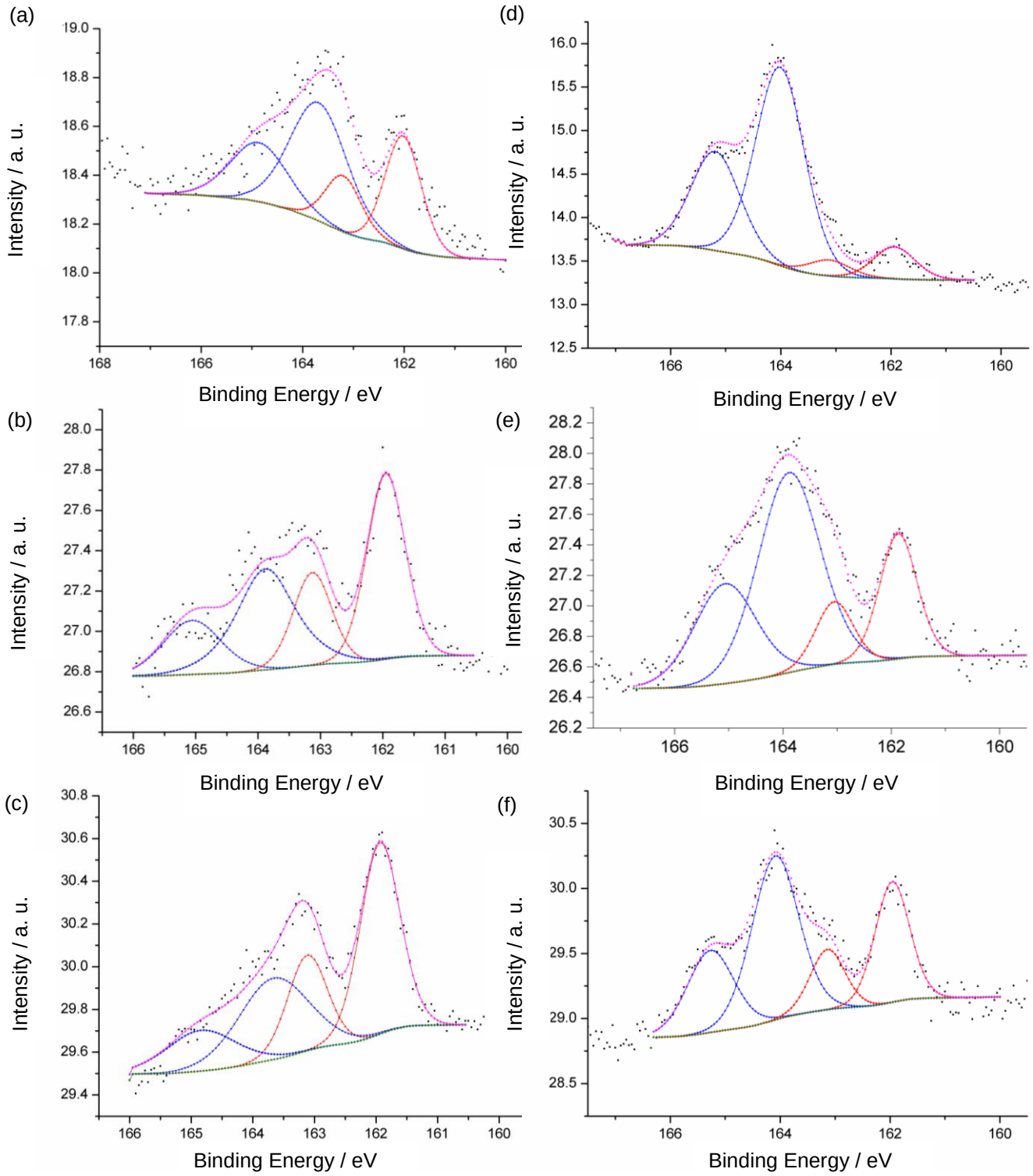

Supplementary Figure 34: The S 2p regions of the high resolution XPS spectra of catenane SAM **1.5**.Cl.Au (left) and, for comparison, thread SAM **16.**Cl.Au (right). XPS spectra acquired at take-off angles (between the sample surface and the energy analyzer) of (a) & (d): 10°, (b) & (e): 40° and (c) & (f): 90°. Raw data (●); fit to the experimental data (●); S 2p S2 (—●—), S 2p S1 (—●—) and background (●). S 2p core level spectra were fitted with a pair of doublets of equal (FWHM), a doublet separation of 1.18 eV, and an S $2p_{3/2}$/S $2p_{1/2}$ peak area ratio of 2:1.

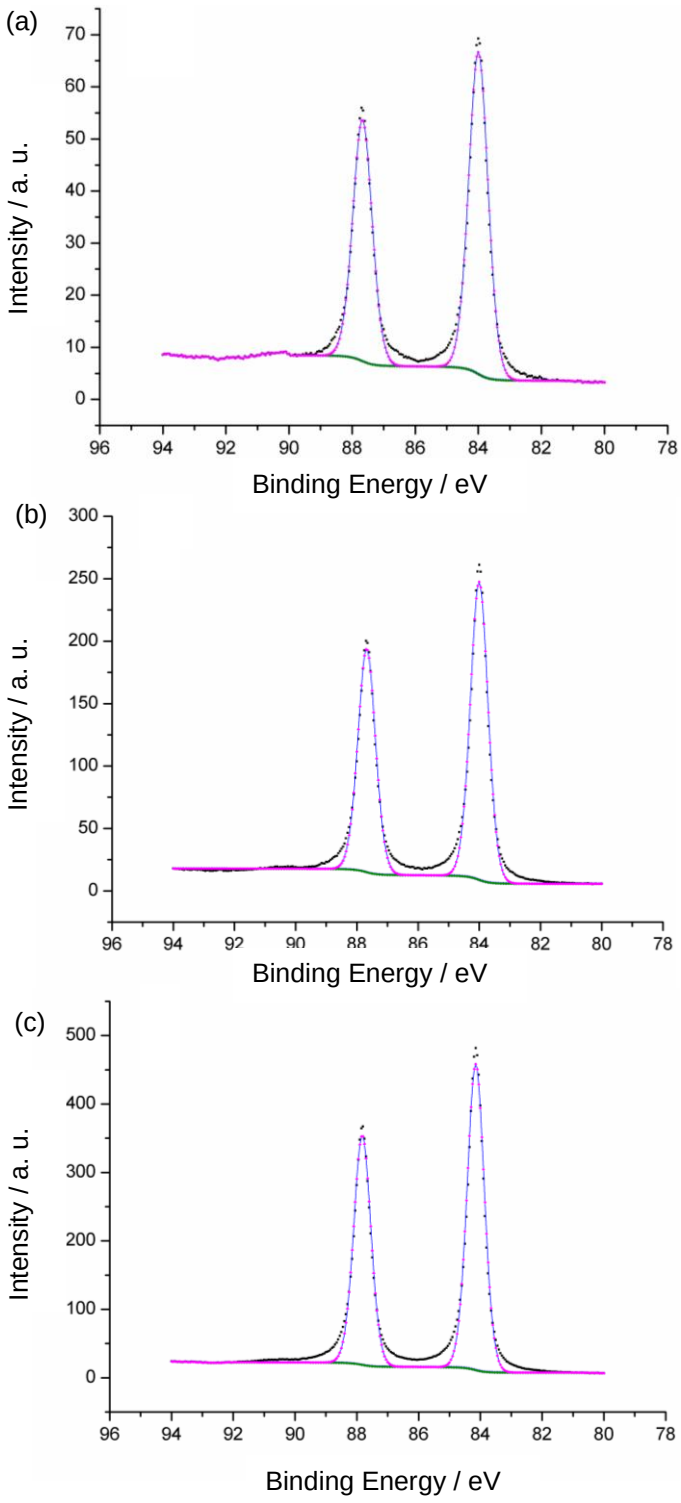

Supplementary Figure 35: The Au 4f regions of the high resolution XPS spectra of catenane SAM **1.5**.Cl.Au. XPS spectra acquired at take-off angles (between the sample surface and the energy analyzer**)** of (a): 10°, (b): 40° and (c): 90°. Raw data (●); fit to the experimental data (●); Au 4f (—●—), and background (●).

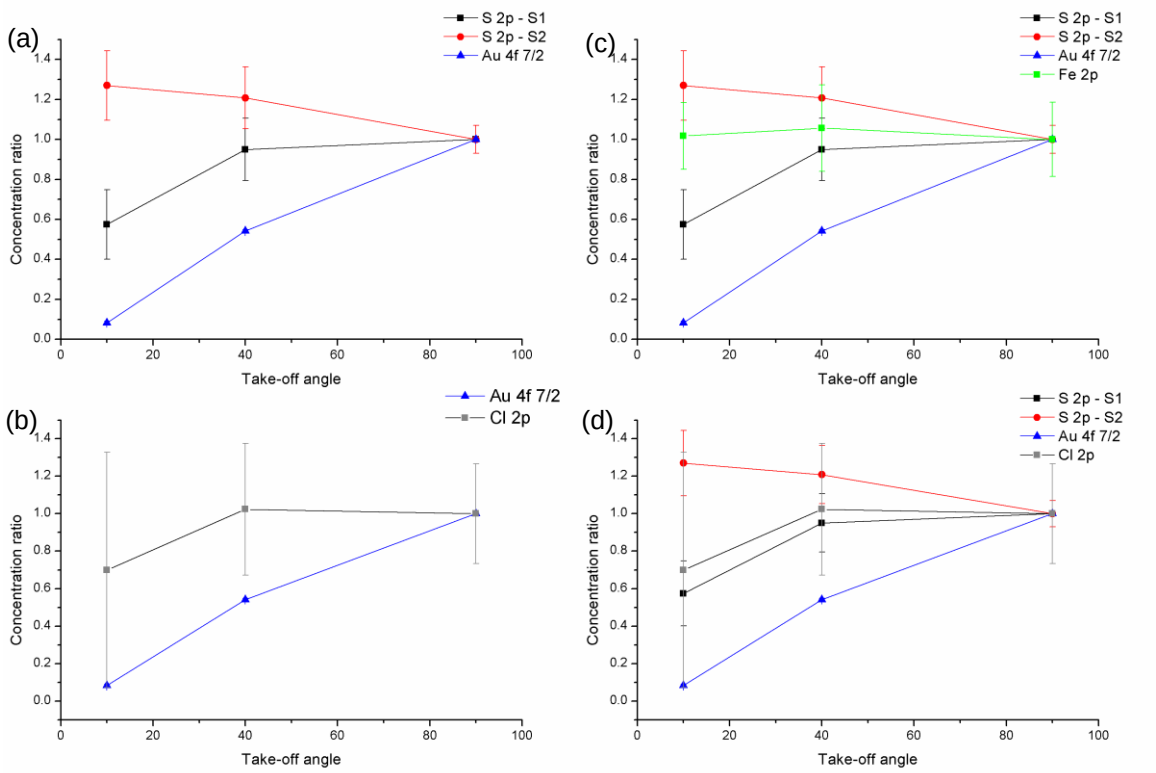

Supplementary Figure 36: Plots of concentration ratio versus take-off angle for catenane SAM **1.5**.Cl.Au: (a) Au 4f, S 2p S1 and S 2p S2; (b) Au 4f and Cl 2p; (c) Au 4f, S 2p S1, S 2p S2 and Fe 2p; (d) Au 4f ,S 2p S1, S 2p S2, Fe 2p and Cl 2p. The concentrations measured at 10° and 45° are divided by the concentrations measured at 90º Concentration ratios (especially at 10°) represent the relative position of the different elements in the monolayer.

Cl and Fe are present in the middle region. As expected thiolate (S1) lies closest to the Au substrate, whilst the free unbound sulfur (S2) is present at the outer surface. XPS measurements were performed on control samples to ensure that the observed Cl 2p peaks were not contamination from the dichloromethane solution: as expected no Cl 2p peaks were observed in the control samples.

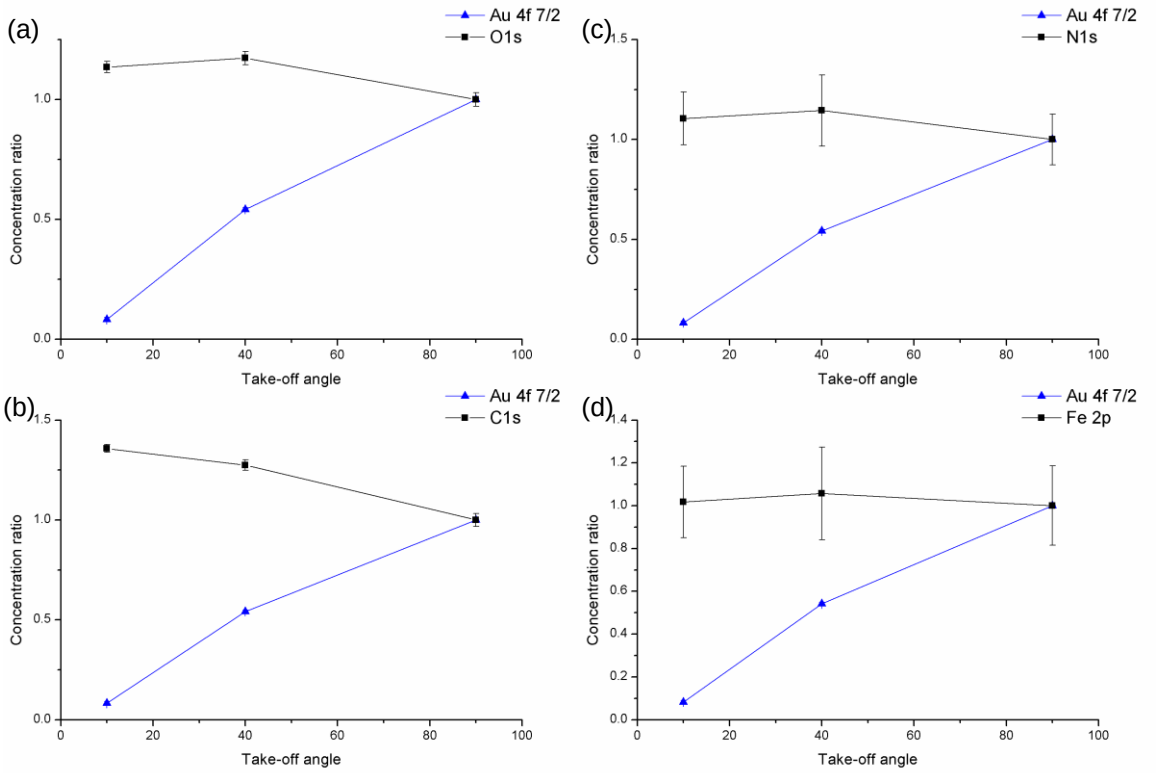

Supplementary Figure 37: Plots of concentration ratio versus take-off angle for catenane SAM **1.5**.Cl.Au: (a) Au 4f and O 1s; (b) Au 4f and C 1s; (c) Au 4f and N 1s; (d) Au 4f and Fe 2p. The concentrations measured at 10° and 45° are divided by the concentrations measured at 90°. Concentration ratios (especially at 10°) represent the relative position of the different elements in the monolayer.

O, N and C are all present in the middle region, i.e. sandwiched between the bound sulfur thiolate and free sulfur thiol.

6) References

1 M. R. Sambrook, P. D. Beer, J. A. Wisner, R. L. Paul and A. R. Cowley, *J. Am. Chem. Soc.*, 2004, **126**, 15364-15365.

2 M. D. Lankshear, N. H. Evans, S. R. Bayly and P. D. Beer, *Chem. - Eur. J.*, 2007, **13**, 3861-3870.

3 L. M. Hancock, L. C. Gilday, S. Carvalho, P. J. Costa, V. Félix, C. J. Serpell, N. L. Kilah and P. D. Beer, *Chem. - Eur. J.*, 2010, **16**, 13082-13094.

4 J. A. Wisner, P. D. Beer and M. G. B. Drew, *Angew. Chem. Int. Ed.*, 2001, **40**, 3606-3610.

5 X. Li, W. Liu, H.-Y. Zhang and B.-L. Wu, *J. Organomet. Chem.*, 2008, **693**, 3295-3302.

6 J. Cosier, and A. M. Glazer, *J. Appl. Cryst.* 1986, **19**, 105-107.

7 Z. Otwinowski and W. Minor, *Processing of X-ray Diffraction Data Collected in Oscillation Mode, Methods Enzymol;* Eds C. W. Carter, R. M. Sweet, Academic Press, 1997, 276.

8 CrysAlisPro, Oxford Diffraction Ltd., Version 1.171.34.41 (release 13-09-2010 CrysAlis171.NET).

9 CrystalClear (Version 2.0, 2009), Rigaku Americas, 9009 TX, USA 77381-5209.

10 A. Altomare, G. Cascarano, C. Giacovazzo, A. Guagliardi, M. C. Burla, G. Polidori and M. Camalli, *J. Appl. Cryst.*, 1994, **27**, 435.

11 L. Palatinus and G. Chapuis, *J. Appl. Cryst.*, 2007, **40**, 786-790.

12 P. W. Betteridge, J. R. Carruthers, R. I. Cooper, K. Prout,and D. J. Watkin, *J. Appl. Cryst.*, 2003, **36**, 1487.

13 (a) A. L. Spek, *J. App. Cryst.*, 2003, **36**, 7-13; (b) P. van der Sluis and A. L. Spek, *Acta Cryst.*, 1990, **A46**, 194-201.

14 M. J. Hynes, *J. Chem. Soc., Dalton Trans.*, 1993, 311-312.

15 J. Tkac and J. J. Davis, *J. Electroanal. Chem.*, 2008, **621**, 117-120.

16 J. C. Hoogvliet, M. Dijksma, B. Kamp and W. P. van Bennekom, *Anal. Chem*., 2000, **72**, 2016-2021.

17 More information can be found at: **www.dl.ac.uk/NCESS/xps/esca300.htm**

18 D. Briggs and M. P. Seah, *Practical Surface Analysis by Auger and X-ray Photo Electron Spectroscopy*, Wiley & Sons, New York, 1983.

19 (a) C. A. Widrig, C. Chung, M. D. Porter, *J. Electroanal. Chem.*, 1991, **310**, 335-359; (b) M. M. Walczak, D. D. Popenoe, R. S. Deinhammer, B. D. Lamp, C. Chung and M. D. Porter, *Langmuir*, 1991, **7**, 2687-2693; (c) D. E. Weisshaar, M. M. Walczak, and M. D. Porter, *Langmuir*, 1993, **9**, 323-329.

20 E. Laviron, *J. Electroanal. Chem.*, 1979, **101**, 19-28.

21 (a) C. van der Marel, M. Yildirim and H. R. Stapert, *J. Vac. Sci. Technol. A*, 2005, **23**, 1456-1470; (b) Angle-resolved measurements - Philips Research, MiPlaza Materials Analysis Publications, *Surface and Thin Film Analysis; X-Ray Photoelectron Spectroscopy (XPS/ESCA).*